

NASA TECHNICAL NOTE

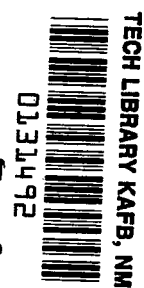


NASA TN D-4502

c.1

NASA TN D-4502

LOAN COPY: RETURN
AFWL (WLIL-2)
KIRTLAND AFB, NM



EXPERIMENTAL INVESTIGATION OF
THE LONGITUDINAL VIBRATION OF A
REPRESENTATIVE LAUNCH VEHICLE
WITH SIMULATED PROPELLANTS

by James A. Schoenster and Robert R. Clary

Langley Research Center

Langley Station, Hampton, Va.





EXPERIMENTAL INVESTIGATION OF THE LONGITUDINAL
VIBRATION OF A REPRESENTATIVE LAUNCH VEHICLE
WITH SIMULATED PROPELLANTS

By James A. Schoenster and Robert R. Clary

Langley Research Center
Langley Station, Hampton, Va.

NATIONAL AERONAUTICS AND SPACE ADMINISTRATION

For sale by the Clearinghouse for Federal Scientific and Technical Information
Springfield, Virginia 22151 - CFSTI price \$3.00

EXPERIMENTAL INVESTIGATION OF THE LONGITUDINAL
VIBRATION OF A REPRESENTATIVE LAUNCH VEHICLE
WITH SIMULATED PROPELLANTS

By James A. Schoenster and Robert R. Clary
Langley Research Center

SUMMARY

The results of an experimental investigation of the longitudinal vibration of a full-scale representative launch-vehicle structure are presented. The vibration characteristics of the vehicle supported upright were determined for frequencies between 5 and 100 hertz by means of force-controlled vibration techniques.

Resonant frequencies, resonant response accelerations, and damping values were determined and the degree of nonresonant vibration was investigated. Static deflections of the propellant tanks due to various levels of simulated propellants were also measured.

The vibration characteristics of the vehicle were influenced by the simulated propellants. The acceleration data were not always sufficient to identify and to separate the various modes of the vehicle. In these cases, a definition of the effect of the contained liquid on the vehicle structure was required for proper association of the modes. In general, there was good agreement between the resonant frequencies selected for detailed study when one source of excitation, two sources of excitation, or the Kennedy-Pancu method of data interpretation were used. However, data obtained from the two sources of excitation and the Kennedy-Pancu plots indicate significant nonresonant amplitude contributions to the total response amplitude obtained with a single source of excitation.

Acoustic resonances of the air column above the liquids in the propellant tanks were detected but did not have a significant effect on the acceleration response of the vehicle containing liquid.

INTRODUCTION

During the development of large complex launch vehicles, a significant amount of effort is directed toward obtaining an understanding of their structural dynamic characteristics. Studies are aimed at determining means of overcoming potential problems such as self-generated instabilities in the guidance and control systems and excessive vibration loadings on the components and payload of the vehicle. These studies have included

experimental investigations of the lateral response of both full-scale vehicles (refs. 1 and 2) and scaled models (refs. 2 and 3); however, very little experimental data have been obtained concerning the longitudinal vibrational responses of large launch vehicles. Considerable interest in obtaining this type of data was generated by a need for a better understanding of the phenomenon called pogo, which caused severe longitudinal oscillations in several launch vehicles including the Thor-Agena (refs. 4 and 5). Pogo is an instability caused by coupling of a longitudinal vibration mode with the dynamics of the propellant feed system and engine operation.

A research program has therefore been undertaken to determine the character of the longitudinal vibrational response of a representative launch vehicle. In reference 6, the results of an experimental and analytical study of the longitudinal vibration of a simplified Thor vehicle structure were described. A subsequent experimental investigation of the vibrational response of the full-scale Thor vehicle with simulated propellants and tank-ullage pressures is reported herein. Included is a description of the testing techniques, the source of excitation, and the effects of nonresonant responses on the forced vibration modes, resonant frequencies, and damping of the structure due to the behavior of the vehicle.

SYMBOLS

| | |
|----------------|--|
| f | frequency, hertz |
| f_n | resonant frequency, hertz |
| Δf | change in frequency, hertz |
| g | acceleration due to gravity, 980.7 centimeters/second ² |
| k | stiffness, newtons/centimeter |
| X, Y, Z | test-vehicle axis system |
| θ | displacement phase angle relative to force, radians |
| $\Delta\theta$ | change in phase angle, radians |

- $\Delta\theta/\Delta f$ change in phase angle as a function of change in frequency of two displacements bounding a resonant frequency and determined from Kennedy-Pancu graphs
- μ twice the ratio of structural damping to critical damping for an equivalent viscous damped system

APPARATUS AND TEST PROCEDURE

Description of Test Vehicle

A structurally complete Thor vehicle (model DM-18A) shown schematically in figure 1 was used in this investigation. The assembly consists of four basic sections: the fuel-tank section, the center-body section, the liquid-oxygen-tank section, and the engine and accessories section. Station numbers are used to identify locations along the length of the vehicle (Z-axis). The diameter of the aft three sections (the engine and accessories section, the liquid-oxygen-tank section, and the center-body section) is 2.44 meters, and the diameter of the fuel-tank section tapers from 2.44 meters at the aft end to 1.90 meters at the forward end. Each section is fastened to its adjacent section or sections with forty 6.35-millimeter (1/4 inch) bolts connecting corresponding attach angles of the involved sections. The assembled vehicle, as shown in figure 2, is approximately 14.5 meters in length.

Some secondary components such as attitude controls and vernier engines were not available for installation and were simulated with mass in the form of lead ballast at various points. These ballast masses and other details of the various sections are shown in figures 3 to 14, and data on the mass and center of gravity are presented in table I.

Details of the fuel tank and its bulkheads are shown in figures 3 to 6. The fuel-tank section (fig. 3) extending from station 151.0 to station 336.0 (fig. 1) is approximately 4.7 meters long. The interior of the fuel tank is shown in figure 4. The wall is of waffle-pattern construction with ring stiffeners and fuel slosh baffles extending around the tank circumference. The interior of the tank is coated with an epoxy compound to retard corrosion (ref. 7).

The forward and aft bulkheads of the fuel tank are shown in figures 5 and 6, respectively. The bulkheads are ellipsoidal with integrally milled reinforcing stiffeners extending radially. Strain gages are attached to each bulkhead. A large-diameter tube is connected to a port on the forward bulkhead for pressurization of the fuel tank. The fuel-transfer-tube attachment is located at the center of the aft bulkhead.

The center-body section (fig. 7) extending from station 336.0 to 369.0 (fig. 1) is approximately 0.84 meter long. This section is of semimonocoque construction with

several ballast weights attached to the sides. It has two hinged access doors, two non-hinged access panels, and several cutouts for tubing and wiring in the wall.

The liquid-oxygen (lox) tank is shown in figures 8 to 10. This section extending from station 369.0 to station 636.7 (fig. 1) is approximately 6.8 meters long. It is formed of two subsections: the liquid-oxygen tank (5.9 meters long) and the liquid-oxygen-tank skirt (0.9 meter long). The subsections are connected by a riveted butt joint at station 602.5. The interior of the liquid-oxygen tank (fig. 8) is of waffle-pattern construction with ring stiffeners at intervals along its length. The fuel-transfer tunnel extends through the liquid-oxygen tank. The interior of the tank is also coated with an epoxy compound to retard corrosion (ref. 7). The forward and aft bulkheads of the liquid-oxygen tank have an ellipsoidal shape with integrally milled reinforcing stiffeners extending radially. The forward bulkhead, with strain gages attached to the outer surface and with plumbing lines for tank pressurization connected to the ports, is shown in figure 9. The center-body section is shown connected to the liquid-oxygen-tank section in this photograph. Also shown is the fuel-transfer tube protruding from the center of the bulkhead. The aft bulkhead and aft skirt of the liquid-oxygen tank are shown in figure 10. Attached to the center of this bulkhead is the lox bellows which connects to one inlet of the turbopump. Protruding from the surface of the bulkhead are the fuel-transfer tube and fuel bellows which connect to the other inlet of the turbopump. Three large gas bottles are mounted on the interior surface of the semimonocoque aft skirt.

The fuel-transfer tube and associated insulation are shown in figure 11. The insulating sections, which are made of glass-fiber laminates and expanded polystyrene, provide both insulation and rigidity to the fuel-transfer tube. This transfer tube is inserted through the liquid-oxygen tank with the aid of the fuel-transfer tunnel shown in figure 8.

The engine and accessories section (figs. 12 to 14) extending from station 636.7 to station 722.0 (fig. 1) is approximately 2.2 meters long. This section is of semimonocoque construction with circumferential stiffeners (figs. 12 and 13). Three thrust beams, constructed of forged and machined fittings and extruded angles and webs, are spaced 120° apart on the wall and extend the length of the section. At the top of these beams are forged thrust fittings that provide the attach locations for the engine assembly. (See fig. 14.)

The engine assembly consists of a large tripod-shaped thrust frame to which the functional elements required to operate the engine are attached. Bracing and attachments for subsystems, which use smaller sections of tubing, are provided. The heaviest items of the functional components are the turbopump, thrust chamber, and gimbal block. The turbopump and associated inlet ports that connect the propellant-feed lines to the turbopump are shown in figure 14. For this series of tests, the thrust chamber was removed

and the excitation and support systems were attached directly to the gimbal block (figs. 12 and 13).

Suspension System

The test vehicle was supported upright along its longitudinal axis on a low-frequency support system (fig. 15). The system was designed to have a minimum effect on the test vehicle while maintaining it at a fixed predetermined elevation. The use of simulated liquid propellants required that the vehicle be supported in an upright, or vertical, position. The vehicle was too heavy to be supported directly on the shaker, and the wide range of propellant conditions precluded the use of interchangeable helical springs. A unique, automatically controlled, air-bellows system was developed to meet the requirements of the suspension system. Lateral restraint was provided by two sets of cables at the upper and lower end of the vehicle. A detailed description of this support system is given in reference 8.

Instrumentation

The instrumentation was designed to provide data necessary to define the longitudinal natural frequencies and mode shapes of the test vehicle. Pressure variations at the top and bottom of both propellant tanks were recorded. The input force to the test vehicle was provided by an electromagnetic vibration exciter and measured by a force gage, which was located between the shaker and the gimbal thrust pad of the vehicle. A servo-oscillator maintained a predetermined constant level of input force.

The primary transducers were lightweight crystal accelerometers and utilized charge amplifier signal conditioning equipment. Pressures were measured by strain-gage-type pressure transducers. Relative strains on the bulkheads of both propellant tanks were also measured. Both the pressure transducers and strain gages used 3-kilocycle carrier signal conditioning equipment.

Shown in figures 16 and 17 are the locations of the accelerometers on the test vehicle. The table in each figure lists the identification number, station number (Z-axis), and radial distance from the center of the vehicle for the accelerometers mounted on the vehicle. The sketches, using the identification number, show the approximate location of these transducers. Pressure transducers were located at both the top and bottom of the two propellant tanks and at the bottom of the fuel-transfer tube. Figures 18 and 19 show the locations of the strain gages on the bottom bulkheads of the fuel and lox tanks. Data were recorded on an FM tape recorder.

Experimental Procedure

The propellant tanks were filled with water in increments, and the change in vehicle mass and change in water height were measured to define the mass in terms of the height of the water in each tank. During this operation, radial static displacement of the lox-tank wall and longitudinal static displacement of the bottom domes of the fuel and lox tanks were measured with dial gages.

Longitudinal response data were obtained while applying ± 1334 newtons of vertical sinusoidal force at the gimbal block. The forcing frequency was varied from 5 to 100 hertz at a constant rate of 0.46 octave/minute (9.4 minutes per sweep). Several frequencies, at which a response was observed from the reaction of the input accelerometer, were selected for more detailed study. Amplitude and phase data were recorded at small increments of frequency about the selected center frequency to obtain a better definition of the peak response. Vehicle resonant response amplitudes were then determined from the output of the various transducers along the length of the vehicle.

Methods of determining normal modes of a structure have been discussed by Lewis and Wrisley (ref. 9), Traill-Nash (ref. 10), and Asher (ref. 11). Their conclusions indicate that for complex structures several sources of excitation are required to obtain normal modes. Due to the lack of adequate attachment locations on the test vehicle, it was impractical to use several sources of excitation as suggested by the referenced reports; however, a second source of excitation was applied at the top of the vehicle to obtain data related to the degree of modal coupling. The second shaker, rated output of ± 222 newtons, was attached to the vehicle at station 151.0 by means of a wooden adapter. Some observed resonant conditions obtained with one shaker were also investigated with two shakers to determine the effects of two sources of vibration on both the resonant frequency and the resonant response accelerations. The force level of the shaker located near the aft end (station 691.1) was held constant at a selected frequency which yielded a 90° phase shift between this applied force and the acceleration at the point of input (station 691.1). The phase of the force output of the second (top) shaker was then adjusted to be in phase or out of phase (depending on the resonant condition being investigated) with that of the force signal from the bottom shaker. The level of force from the top shaker was then increased until a 90° phase shift was obtained between this force and the resulting acceleration at its point of application. Adjustments of the frequency of both shakers and the force level at the top shaker were necessary to obtain the desired phase relationships. After satisfactory excitation conditions were achieved, the resonant response accelerations were determined. The data from this study are reported only for tests with the empty test vehicle.

The test configurations are listed in table II. This table gives both pressurized (denoted by P in vehicle configuration designation) and unpressurized vehicle conditions.

Damping was determined by means of the method of Mead (ref. 12) and Pendered and Bishop (ref. 13) as applied to data obtained from Kennedy-Pancu graphs (ref. 14). The damping factor μ was calculated from

$$\mu = \frac{2}{f_n \frac{\Delta\theta}{\Delta f}} \quad (1)$$

where μ is twice the ratio of damping to critical damping for an equivalent viscous damped system, $\frac{\Delta\theta}{\Delta f}$ is the slope of the phase angle in radians with respect to frequency in hertz at the resonant frequency determined from the "best circle" of the Kennedy-Pancu plots, and f_n is the resonant frequency in hertz.

PRESENTATION OF EXPERIMENTAL DATA

Vibration and static data are presented in table III, table IV, and figures 20 to 32. A brief explanation is provided for each of the methods used to present the data.

Resonant Frequencies

Figure 20 presents a summary of selected resonant frequencies as a function of the total vehicle mass. Curves are faired through frequency data points for which mode shapes exhibit similar characteristics. Table III presents the experimentally obtained acoustic resonant frequencies in the air column above the liquid in both propellant tanks and the acoustic resonant frequencies calculated by using the frequency equation for the vibration of an air column (ref. 15, p. 584).

Frequency Response

Frequency response curves of the thrust-frame acceleration at the location of the input force (station 691.1) and the turbopump acceleration for all pressurized configurations are presented in figure 21. Longitudinal accelerations at various locations along the length of the vehicle, pressures at the bottom of the fuel and liquid-oxygen tanks, and relative strains at each of the two locations on the bottom bulkheads of the fuel and liquid-oxygen tanks are presented in figures 22(a), 22(b), and 22(c), respectively, for a typical test condition (configuration 6P). The strains were normalized to an arbitrary level to show the relative values. The response of the thrust frame at station 691.1 is shown in figures 22(b) and 22(c) for reference.

Resonant Response Accelerations

Normalized acceleration responses are presented for several vehicle configurations (both pressurized and unpressurized) in figures 23 to 27. Measured accelerations

normalized by the acceleration at station 691.1 are shown as a function of the nondimensional vehicle length. In figures 24 to 27, the sketches at the right of the figure indicate the direction of the forces of the liquid masses on the bottom bulkhead of each tank relative to the structural forces at the ends of the vehicle. The directions of the forces of the liquid masses were determined from the outputs of the pressure transducers located in the tanks.

Nonresonant Response and Damping

Kennedy-Pancu method.- The effects of nonresonant contributions on the resonant response of the vehicle were studied by using the method of data interpretation suggested by reference 14. The graphs shown in figures 28(a) and 28(b) are Kennedy-Pancu plots (ref. 14) around the 29.5-hertz and 45.8-hertz resonant frequencies for configuration 6P, with station 691.1 as a typical example. This method of interpreting experimental data utilizes both amplitude and phase measurements to separate the normal mode response at a particular resonant frequency from the total response at that frequency. Amplitude and phase data are plotted on polar coordinates for small increments of frequency and a "best circle" is fitted to the data points from which a maximum change in the length of the circular arc with respect to a change in frequency is distinguishable. A diameter drawn perpendicular to the force phase reference should pass through the point at which a maximum change in the circular-arc length with respect to a frequency change occurs. The intersection of this diameter and the circle locates the resonant frequency, and the intersection of the circle and the opposite end of this diameter locates the displaced origin.

Normal mode amplitudes and damping factors are obtained from measurements taken with respect to the displaced origin. The distance between the displaced origin and the actual origin represents the nonresonant response. In figure 28, the radial amplitude is the ratio of the displacement (determined from acceleration measurements) to the input force and the phase angle is the angle between the displacement and force. The best circle was fitted to the data and this resulted in the normal mode response being represented by the diameter JH and the nonresonant response being represented by the distance OJ. The slope of the phase angle with respect to frequency $\frac{\Delta\theta}{\Delta f}$ used in equation (1) to determine damping is obtained from $\Delta\theta$ (fig. 28) and a selected value of Δf (0.2 hertz for this example). The selection of Δf is based on the assumptions of Mead (ref. 12).

The resonant frequencies and damping values listed in table IV for some modes of several configurations were determined from plots similar to the ones presented in figure 28. Further discussion of this method of data interpretation may be found in references 13, 14, 16, and 17.

Two-shaker excitation.- Data for comparison of two-shaker excitation with one-shaker excitation are presented for the empty vehicle in figure 29. Since it was necessary

to use a large adapter (85.4 kilograms) to attach the additional shaker at the top of the vehicle, the mode shapes compared are those obtained with the second shaker removed but with frame in place and those obtained with both shakers operating.

Static Tests

The data obtained during the loading of the propellant tanks with simulated propellants are shown in figures 30 to 32. Presented in figure 30 are the diametrical deflections at stations 408, 492, and 576 as a function of the level of water in the liquid-oxygen tank. Deflections of the bottom bulkheads at the center of the dome and the quarter-point of the dome (i.e., halfway between the center and the outer edge of the dome) of the liquid-oxygen tank (fig. 31) and the fuel tank (fig. 32) are presented as a function of simulated propellant mass in the respective tanks.

RESULTS AND DISCUSSION

The vibration response characteristics of the full-scale test vehicle were determined for several vehicle configurations by means of force-controlled vibration techniques. Resonant response accelerations, damping values, and resonant frequencies were determined for each of the vehicle configurations under the simulated free-free boundary conditions. In addition, an investigation into the degree of nonresonant vibration contributions to the resonant response was performed. Static deflections of the propellant tanks due to various levels of simulated propellants are also discussed.

Resonant Frequencies

Shown in figure 20 is the variation of frequency with vehicle mass of five resonant responses. These responses have been designated mode A, mode B, mode C, lox-tank acoustic resonance, and fuel-tank acoustic resonance. Mode A appears to be a simple tension-compression mode of the vehicle in which the ends of the vehicle are moving out of phase with respect to each other. Modes B and C are associated with the motion of the liquid in the vehicle and cannot be described as simply as mode A. Further discussion about the shape of these modes is presented later. A decrease in frequency with increasing liquid mass occurs for both modes A and B, as would be anticipated for a dynamic system to which mass was added. However, mode C is independent of the liquid mass and remains relatively constant at $f_n = 45$ hertz. This type of response suggests the presence of a cantilevered mass whose response frequency (45 hertz) is not coupled with that of the supporting structure.

It was possible to determine experimentally the trends of modes A, B, and C for the vehicle with varying propellant level although it was not possible to relate these modes

with any of the modes for the empty vehicle. The acoustic-mode frequency trends could be traced to the empty vehicle and were dependent only on the distance between the liquid surface and the top bulkhead of the tank in which the liquid was contained.

The frequencies of the empty vehicle are in general agreement with those frequencies shown in the longitudinal impedance plots of reference 6 for an unpressurized Thor vehicle having both the oxygen and the fuel tanks closed. Most of the resonant frequencies in reference 6 are slightly higher than those obtained during the present series of tests, but this may be attributed to the 17-percent increase in mass of the test vehicle used. However, the 28-hertz and 34.5-hertz resonant frequencies identified as acoustic frequencies in the lox tank and fuel tank, respectively, agree very closely with the 27.7-hertz and 34.0-hertz frequencies given in reference 6.

Frequency Response

Initial determination of the resonant response frequencies of the vehicle was selected from frequency response plots obtained at several stations along the length for a constant force input. The acceleration response of the thrust frame at station 691.1 (location of the applied force) shows several distinct peaks for each of the various vehicle configurations (fig. 21(a)). The frequencies at which resonances were identified and reported are indicated by the appropriate symbols. Generally, it may be noted that although the amplitudes for modes B and C are associated with peaks in the response curves, the response at mode A frequencies for the higher mass configurations are not clearly defined. The acceleration response curves for the turbopump (fig. 21(b)) also show a complex response similar to that measured at station 691.1.

Although some of the resonant frequencies may be easily selected by observing peaks in the response curves, such as the 29.5-hertz and 45.8-hertz resonant frequencies for configuration 6P (fig. 21(a)), in many cases it would be difficult to select one frequency from the several responses which appear at close intervals in the response curves, such as 45 hertz as the resonant frequency of interest for configuration 7P. Responses at other locations along the length of the vehicle also indicate that the same difficulties would be present in selecting the resonant frequencies from those plots. The response at several locations on the vehicle for configuration 6P (fig. 22) may serve as an example. In figure 22(a), peaks in the acceleration response for the mode A frequency of 15.5 hertz were observed at stations 151.0, 336.0, and 369.0 but were not evident at stations 636.4, 691.1, and 720.0. However, the resonant frequency for mode C would be difficult to select from the highly fluctuating responses at stations 151.0, 336.0, and 369.0. Many of these peaks are possibly attributed to the response of small components near the transducer which have a resonant frequency in the immediate frequency range of interest.

The response curves determined from liquid pressure transducers on the bottom bulkheads of both the fuel and lox tanks of vehicle configuration 6P are presented in figure 22(b). The pressure reached peak values very close to frequencies identified as resonant frequencies by peaks in the acceleration response curves for modes B and C. In addition, peaks appeared at the mode A frequencies which were not observable in the acceleration response at station 691.1. Also, the response of the strain gages (fig. 22(c)) showed peak values close to the mode A, mode B, and mode C frequencies. Although the exact motion of the propellants is not known, the frequency response curves indicate that their effect is closely associated with the dynamics of the structure. Therefore, these data contribute to the definition of the resonant response of the test vehicle.

The acoustic frequencies were clearly identified by peaks in the response plots of air pressure measured at the top of the bulkhead in each of the two propellant tanks. The effect of these acoustic resonances on the structural accelerations at station 691.1 is shown in figure 21(a). Only data from the empty vehicle exhibit significant peaks in the acceleration response curves and, with the exception of those of configuration 4P, the acoustic-mode frequencies would probably go unnoticed in the response curves. Even for configuration 4P, a noticeable peak occurs only at the resonant frequency of the air column in the lox tank. A similar observation is made upon inspection of the acceleration response curves for the turbopump (fig. 21(b)). The acceleration response along the length of the vehicle, the pressures at the bottom bulkheads, and the strains in the bottom bulkheads do not indicate a strong response at the acoustic frequencies.

Resonant Response Accelerations

The resonant response accelerations for the four modes (excluding acoustic modes) of the empty vehicle are presented in figure 23. The mode shapes are very similar. Only for $f_n = 79.8$ hertz is a phase difference indicated between the motion of one of the major components of the structure and the motion of the structure itself. The motion of the turbopump is out of phase for this resonant frequency. However, for the next resonant frequency ($f_n = 88$ hertz) the turbopump motion is again in phase with the motion of the aft end of the vehicle. Several additional measurements were made at various locations on the vehicle, such as the end of the fuel-transfer tube and the engine gas bottles, but experimental evidence that would explain the differences between resonances at 54.0, 62.5, and 88.0 hertz was not obtained.

The resonant response accelerations for modes A and C of configurations 2 and 2P and of configurations 3 and 3P are presented in figures 24 and 25, respectively; those for modes B and C of configurations 6 and 6P and of configurations 9 and 9P are given in figures 26 and 27, respectively. The structural resonant response accelerations associated with mode A were not determined for the greater mass configurations because of the

inability of the accelerometers to detect the very low acceleration levels associated with these modes. However, it was possible to relate the response at the mode A frequencies by observing the relative phases of the forces of the propellants on their respective bulkheads. For mode A responses, the motions of opposite ends of the vehicle are out of phase with each other and the forces developed by the fluids in the propellant tanks are in phase with forces developed by the adjacent structures. Therefore, the force developed by the fluid in the fuel tank is out of phase with that developed in the liquid-oxygen tank.

The structural resonant response accelerations at the mode B and C frequencies are similar in shape; neither acceleration has an apparent nodal point along the length of the structure. The motion of the aft end of the vehicle is somewhat higher in mode C than in mode B, but motions at all stations along the length of the vehicle are in phase with each other. A comparison of fluid forces indicates the difference between modes B and C and provides data demonstrating the necessary balance of forces required for equilibrium. For mode B, the force generated by the liquid in the lox tank is in phase with that generated by the adjacent structure while the force generated by the liquid in the fuel tank is out of phase with forces generated by the structure and the simulated liquid oxygen. For mode C the forces generated by the liquids in the two tanks are out of phase with those generated by the adjacent structures. None of the three experimentally determined modes could be related to the modes determined for the empty vehicle. Mode C, being independent of vehicle mass and having a relatively large amplitude in the thrust-frame area of the vehicle, may be associated with the dynamics of the attachment of the thrust frame to the structure. In reference 6 the resonant frequency of the thrust frame was found to be 55 hertz when independently excited on the empty test vehicle. It is conceivable that the mass of propellant on the turbopump structure of this section could cause a drop in resonant frequency to approximately 45 hertz.

The resonant-response accelerations for the unpressurized vehicle agree with those of the pressurized vehicle (figs. 24 to 27). In general, the resonant frequency is slightly higher for the pressurized vehicle but in none of the observed modes is it more than 9 percent.

Nonresonant Response and Damping

Kennedy-Pancu method.- The damping factors and resonant frequencies determined from the Kennedy-Pancu plots are given in table IV for configurations 2P, 3P, 6P, and 9P. The resonant frequencies determined by this method are in close agreement with those determined by the peak amplitude method using a single shaker. The damping obtained from mode C was relatively constant with respect to the vehicle mass. A similar observation cannot be made for modes A and B.

Resonant frequencies and damping factors obtained from the use of Kennedy-Pancu graphs illustrated in figure 28 are presented for modes B and C of configuration 6P. The "best circle" for both modes was fitted through at least five data points which are spaced at increments of 0.2 hertz. The frequency at which data were obtained closest to the major diameter JH is selected to be the resonant frequency. Both plots indicate that there were some nonresonant responses OJ to the experimentally measured amplitudes. For mode B the experimentally measured amplitude at $f_n = 29.5$ hertz is slightly less than the "normal mode amplitude" JH, whereas for mode C the experimentally measured amplitude at $f_n = 45.8$ hertz is greater than the normal mode amplitude. It should also be noted that the resonant frequency does not occur for either mode at the quadrature response frequency but at relative phase angles greater than 90° for mode C and less than 90° for mode B. Data obtained from other transducers located along the length of the vehicle yielded similar results, but the ratio of nonresonant amplitude to normal mode amplitude increased considerably. This relative increase in amplitude of the nonresonant vibration, as determined from the Kennedy-Pancu graphs, would raise doubts about the use of the assumption that the phase and amplitude of the nonresonant vibration remain constant over the frequency range of resonance investigation. For the empty-vehicle configuration, values of damping were not calculated because this ratio of nonresonant amplitude to normal mode amplitude was high (greater than 1).

Two-shaker excitation.- In addition to the large shaker at the bottom of the vehicle, a second shaker was attached to the top of the vehicle for some tests. With the two shakers, the proper phase relationships for only three resonant responses of the empty vehicle could be obtained. None of the resonant responses of the vehicle with liquid in the tanks could be adjusted to obtain the proper phase relationships. The three modes for the empty vehicle with the large adapter attached were at $f_n = 60.5, 80.3,$ and 88.0 hertz. In figure 29 are presented the resonant response accelerations obtained by using one shaker and two shakers. With two-shaker excitation the amplitude at the top of the vehicle increased considerably at $f_n = 60.5$ hertz and 88.0 hertz, but little change was noticed at other frequencies. The involved frequencies were affected by less than 1 hertz. The resonant response accelerations at 80.3 hertz were relatively unaffected by the introduction of the second shaker. These data would indicate that the resonant response accelerations at 60.5 hertz and 88.0 hertz are strongly coupled amplitudes rather than the normal mode amplitudes that analysis might predict. Measurements of the exact phase angles, which seldom were exactly 90° or 270° phase difference referenced to the input force, also indicated that the measured amplitudes did not yield normal mode amplitudes.

Static Tests

The loading of the tank with simulated propellants caused little change in the liquid-oxygen-tank diameter at the top (station 408) along either the X- or Y-axis (fig. 30). The diametrical deflections in the middle of the tank (station 492) become significant only after the level of water is above that station and thereafter the deflections appear linear. The change in diameter at the bottom of the tank (station 576) increased approximately linearly along both the X- and Y-axes with increased propellant level and reached a maximum of 0.0165 centimeter for the X-axis and 0.127 centimeter for the Y-axis.

Deflections of the bottom dome of the liquid-oxygen tank (fig. 31) show that the stiffness of the dome is approximately linear over the mass conditions investigated. The stiffness determined from the slope of the faired curve through data taken at the center of the bulkhead is 1.9×10^6 newtons/centimeter and that determined from the slope of the faired curve through data taken at the quarter-point is 3.5×10^6 newtons/centimeter.

The deflection data for the bottom fuel-tank bulkhead exhibited the same linear characteristics (fig. 32), over the mass conditions investigated, but the maximum deflections occurred at the quarter-point and not at the center of the bulkhead. The stiffness determined from the slope of the faired curve through data taken at the center of the bulkhead is 2.2×10^6 newtons/centimeter and that determined from the slope of the faired curve through data taken at the quarter-point is 1.0×10^6 newtons/centimeter. This difference can be partially explained by the manner of construction of the fuel tank, which has the fuel-transfer tube connected at the center of the bottom bulkhead. This tube has sections of insulation wrapping where it passes through a tunnel in the liquid-oxygen tank, as indicated in figure 10. These fabricated sections enclose the tube for approximately 6.71 meters and can provide a resultant restraint to the center of the dome.

CONCLUSIONS

An experimental investigation has been conducted on a representative full-scale launch vehicle to study its vibration characteristics under longitudinal excitation. The vehicle was investigated with various liquid loadings and two propellant-tank ullage pressures. The conclusions of this investigation are stated as follows:

1. The vibrational response of the vehicle was significantly influenced by the contained liquids. Proper identification and association of the modes were made by obtaining data on the effects of the contained liquid, such as pressure and bulkhead strain, in addition to the effects of accelerations along the length of the vehicle. Because acceleration data alone did not completely identify the vehicle resonant responses, association between the modes of the empty vehicle and the modes of the vehicle with contained liquids, with the exception of the acoustic modes, could not be made.

2. In general, there was good agreement between the resonant frequencies selected for detailed study when one source of excitation, two sources of excitation, and the Kennedy-Pancu method of data interpretation were used. However, both the Kennedy-Pancu method and the two-shaker method indicated that a significant amount of nonresonant vibration was included in the measured resonant response accelerations obtained with a single source of vibration excitation.

3. The resonant frequencies of the air column (acoustic resonances) above the liquid in both the liquid-oxygen tank and the fuel tank were dependent only on the height of the air column and did not significantly affect the acceleration response of the vehicle for the various mass configurations investigated.

4. Propellant-tank pressurization tended to increase the resonant frequencies slightly but did not appreciably affect the resonant response shapes.

5. The modal damping of the vehicle was relatively constant with respect to vehicle mass for the resonant response whose frequency remained constant with respect to the vehicle mass (mode C).

6. The static longitudinal deflections at the bottom bulkhead of both propellant tanks and the diametrical deflection near the bottom of the liquid-oxygen tank increased linearly with increasing propellant mass in the tanks.

Langley Research Center,
National Aeronautics and Space Administration,
Langley Station, Hampton, Va., December 7, 1967,
124-08-05-19-23.

REFERENCES

1. Leadbetter, Sumner A.; Alley, Vernon L., Jr.; Herr, Robert W.; and Gerringer, A. Harper: An Experimental and Analytical Investigation of the Natural Frequencies and Mode Shapes of a Four-Stage Solid-Propellant Rocket Vehicle. NASA TN D-1354, 1962.
2. Mixson, John S.; and Catherine, John J.: Comparison of Experimental Vibration Characteristics Obtained From a 1/5-Scale Model and From a Full-Scale Saturn SA-1. NASA TN D-2215, 1964.
3. Leadbetter, S. A.; and Raney, J. P.: Analytical and Experimental Studies of the Dynamics of Launch Vehicles. AIAA Symposium on Structural Dynamics and Aeroelasticity, Aug.-Sept. 1965, pp. 523-527.
4. Aerospace Syst. Eng.: Briefing Charts Thor 20 cps Study. Rept. SM-44160 (Contract AF 04(695)-274), Missile & Space Syst. Div., Douglas Aircraft Co., Inc., July 1963.
5. Davis, W. F.; Keeton, D. L.; and Lynch, T. F.: Thor Longitudinal Oscillation Study. Rept. SM-45009, Missile & Space Syst. Div., Douglas Aircraft Co., Inc., Mar. 1964. (Available from DDC as AD-460911.)
6. Carden, Huey D.; and Raney, John P.: An Experimental and Analytical Study of the Longitudinal Vibration of a Simplified Thor Vehicle Structure. NASA TN D-3632, 1966.
7. Powell, Clemans A., Jr.; and Scholl, Harland F.: Corrosion Problems With Simulated Fuel in Launch Vehicle Models. Mater. Protect., vol. 5, no. 8, Aug. 1966, pp. 33-34.
8. Schoenster, James A.; Pearson, Jerome; and Dixon, Grayson V.: A Unique Suspension System for Longitudinal Vibration Testing of Large Launch Vehicles. Shock Vib. Bull., Bull. 35, Pt. 2, U.S. Dept. Defense, Jan. 1966, pp. 191-196.
9. Lewis, Robert C.; and Wrisley, Donald L.: A System for the Excitation of Pure Natural Modes of Complex Structure. J. Aeron. Sci., vol. 17, no. 11, Nov. 1950, pp. 705-722, 735.
10. Traill-Nash, R. W.: On the Excitation of Pure Natural Modes in Aircraft Resonance Testing. J. Aero/Space Sci., vol. 25, no. 12, Dec. 1958, pp. 775-778.
11. Asher, Gifford W.: A Method of Normal Mode Excitation Utilizing Admittance Measurements. Proceedings of the National Specialists Meeting on Dynamics and Aeroelasticity, Inst. Aeron. Sci., Nov. 1958, pp. 69-76.
12. Mead, D. J.: The Internal Damping Due to Structural Joints and Techniques for General Damping Measurement. C.P. No. 452, Brit. A.R.C., 1959.

13. Pendered, J. W.; and Bishop, R. E. D.: A Critical Introduction to Some Industrial Resonance Testing Techniques. *J. Mech. Eng. Sci.*, vol. 5, no. 4, 1963, pp. 345-367.
14. Kennedy, Charles C.; and Pancu, C. D. P.: Use of Vectors in Vibration Measurement and Analysis. *J. Aeron. Sci.*, vol. 14, no. 11, Nov. 1947, pp. 603-625.
15. Hausmann, Erich; and Slack, Edgar P.: *Physics*. Third ed., D. Van Nostrand Co., Inc., c.1948.
16. Bishop, R. E. D.; and Johnson, D. C.: *The Mechanics of Vibration*. Cambridge Univ. Press, 1960.
17. Bishop, R. E. D.; and Gladwell, G. M. L.: An Investigation Into the Theory of Resonance Testing. *Phil. Trans. Roy. Soc., London, ser. A*, vol. 255, no. 1055, Jan. 17, 1963, pp. 241-280.

TABLE I.- TEST VEHICLE EXPERIMENTAL MASSES

| Sections of vehicle structure | | | Components included in section | | |
|--|------------------------|--|--------------------------------|----------|--------------------------------|
| Item | Total section mass, kg | Section center of gravity at station - | Item | Mass, kg | Center of gravity at station - |
| Engine and accessories section (figs. 12 to 14) | 1135.7 | 669.4 | 11 lead plates | 133.8 | 695.0 |
| | | | Adapter plate | 20.3 | 688.0 |
| Liquid-oxygen tank (figs. 8 to 10) | 770.4 | 519.3 | Bellows extension (fuel) | 11.1 | ^a 629.7 |
| | | | Bellows extension (lox) | 4.7 | ^a 635.0 |
| | | | Gas bottles | 61.7 | ^a 620.0 |
| | | | Pressure-plumbing lines | 8.8 | ^a 350.0 |
| | | | Fuel-transfer tube | 15.9 | 496.9 |
| | | | Fuel-transfer tube insulation | 24.9 | ^a 496.9 |
| Center-body section (fig. 7) | 148.0 | 341.8 | 6 lead plates | 55.5 | 351.7 |
| Fuel tank (figs. 3 to 6) | 409.6 | 253.0 | Pressure-plumbing lines | 4.4 | 142.0 |
| Total mass of sections: 2463.7 kg at c.g. station 534.2 | | | | | |
| Total mass of assembled vehicle: 2464.4 kg at c.g. station 534.4 | | | | | |

^aEstimated.

TABLE II.- VEHICLE CONFIGURATION DATA

| Configuration | Vehicle mass, kg | Simulated liquid oxygen | | Simulated fuel | | aTotal mass, kg |
|---------------|------------------|-------------------------|-----------------------------|----------------|-----------------------------|-----------------|
| | | aMass, kg | Pressure, N/cm ² | aMass, kg | Pressure, N/cm ² | |
| 1 | 2463 | ----- | --- | ----- | --- | 2 465 |
| 2 | 2463 | 2 720 | --- | 1 450 | --- | 6 635 |
| 3 | 2463 | 6 805 | --- | 3 630 | --- | 12 900 |
| 4 | 2463 | 9 435 | --- | 5 035 | --- | 16 935 |
| 5 | 2463 | 12 110 | --- | 6 485 | --- | 21 060 |
| 6 | 2463 | 14 650 | --- | 7 815 | --- | 24 930 |
| 7 | 2463 | 17 645 | --- | 9 435 | --- | 29 545 |
| 8 | 2463 | 20 640 | --- | 11 000 | --- | 34 105 |
| 9 | 2463 | 23 675 | --- | 12 610 | --- | 38 750 |
| 2P | 2463 | 2 720 | 10.4 | 1 450 | 8.5 | 6 635 |
| 3P | 2463 | 6 805 | 10.4 | 3 630 | 8.5 | 12 900 |
| 4P | 2463 | 9 435 | 10.4 | 5 035 | 8.5 | 16 935 |
| 5P | 2463 | 12 110 | 10.4 | 6 485 | 8.5 | 21 060 |
| 6P | 2463 | 14 650 | 10.4 | 7 815 | 8.5 | 24 930 |
| 7P | 2463 | 17 645 | 10.4 | 9 435 | 8.5 | 29 545 |
| 8P | 2463 | 20 640 | 10.4 | 11 000 | 8.5 | 34 105 |
| 9P | 2463 | 23 675 | 10.4 | 12 610 | 8.5 | 38 750 |

aMass to nearest 5 kilograms.

TABLE III.- ACOUSTIC FREQUENCIES IN THE PROPELLANT TANKS

| Configuration | Liquid-oxygen tank | | Fuel tank | |
|---------------|--------------------------|----------------------------|--------------------------|----------------------------|
| | Calculated frequency, Hz | Experimental frequency, Hz | Calculated frequency, Hz | Experimental frequency, Hz |
| 1 | 28.3 | 28.0 | 35.6 | 34.5 |
| 2P | 30.6 | 30.5 | 36.8 | 36.0 |
| 3P | 36.4 | 36.0 | 41.2 | 40.5 |
| 4P | 41.5 | 41.5 | 44.9 | 45.0 |
| 5P | 48.5 | 47.5 | 49.6 | 49.0 |
| 6P | 58.0 | 57.5 | 55.0 | 55.0 |

TABLE IV.- RESONANT FREQUENCIES AND DAMPING FACTORS
FROM KENNEDY-PANCU PLOTS

| Mode | Configuration 2P | | Configuration 3P | | Configuration 6P | | Configuration 9P | |
|------|------------------|-----------------------|------------------|-----------------------|------------------|-----------------------|------------------|-----------------------|
| | Frequency, Hz | Damping factor, μ |
| A | 32.5 | 0.029 | 23.4 | 0.019 | --- | ---- | --- | ---- |
| B | --- | ---- | --- | ---- | 29.5 | 0.080 | 19.6 | 0.044 |
| C | 45.4 | 0.027 | 44.7 | 0.023 | 45.8 | 0.030 | 45.6 | 0.027 |

Station 722.0 636.7 602.5 369.0 336.0 151.0

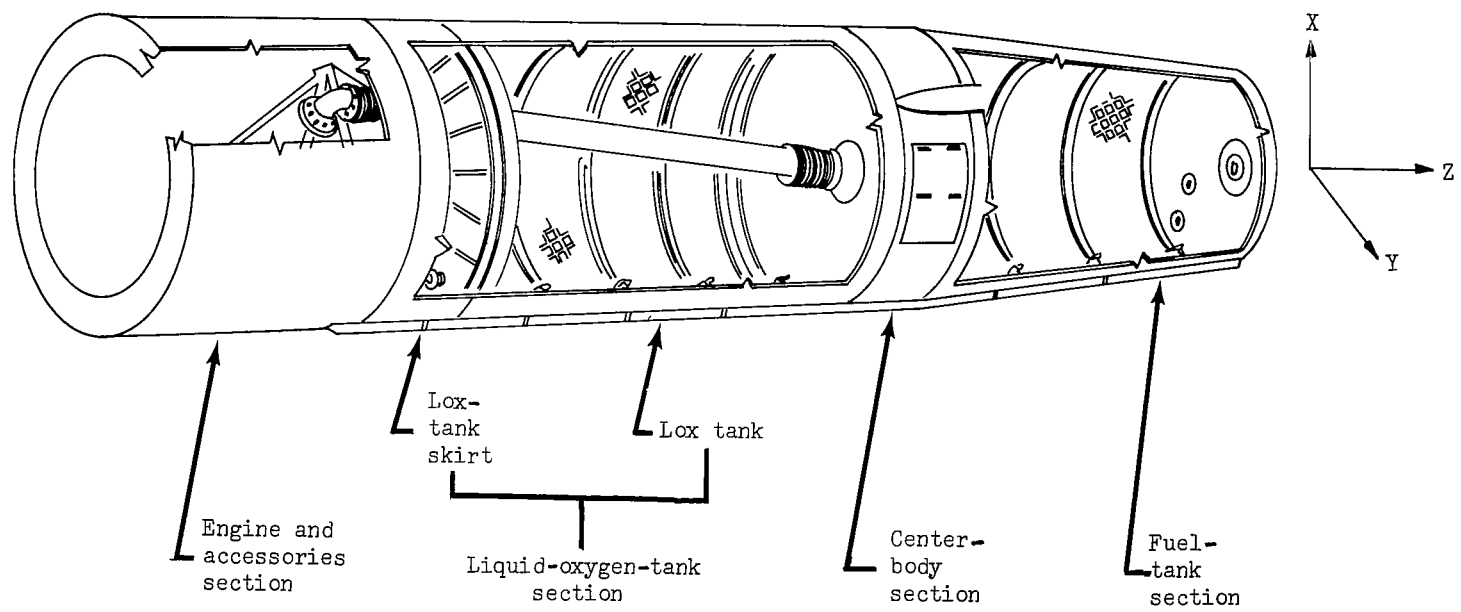


Figure 1.- Schematic cutaway of test vehicle.

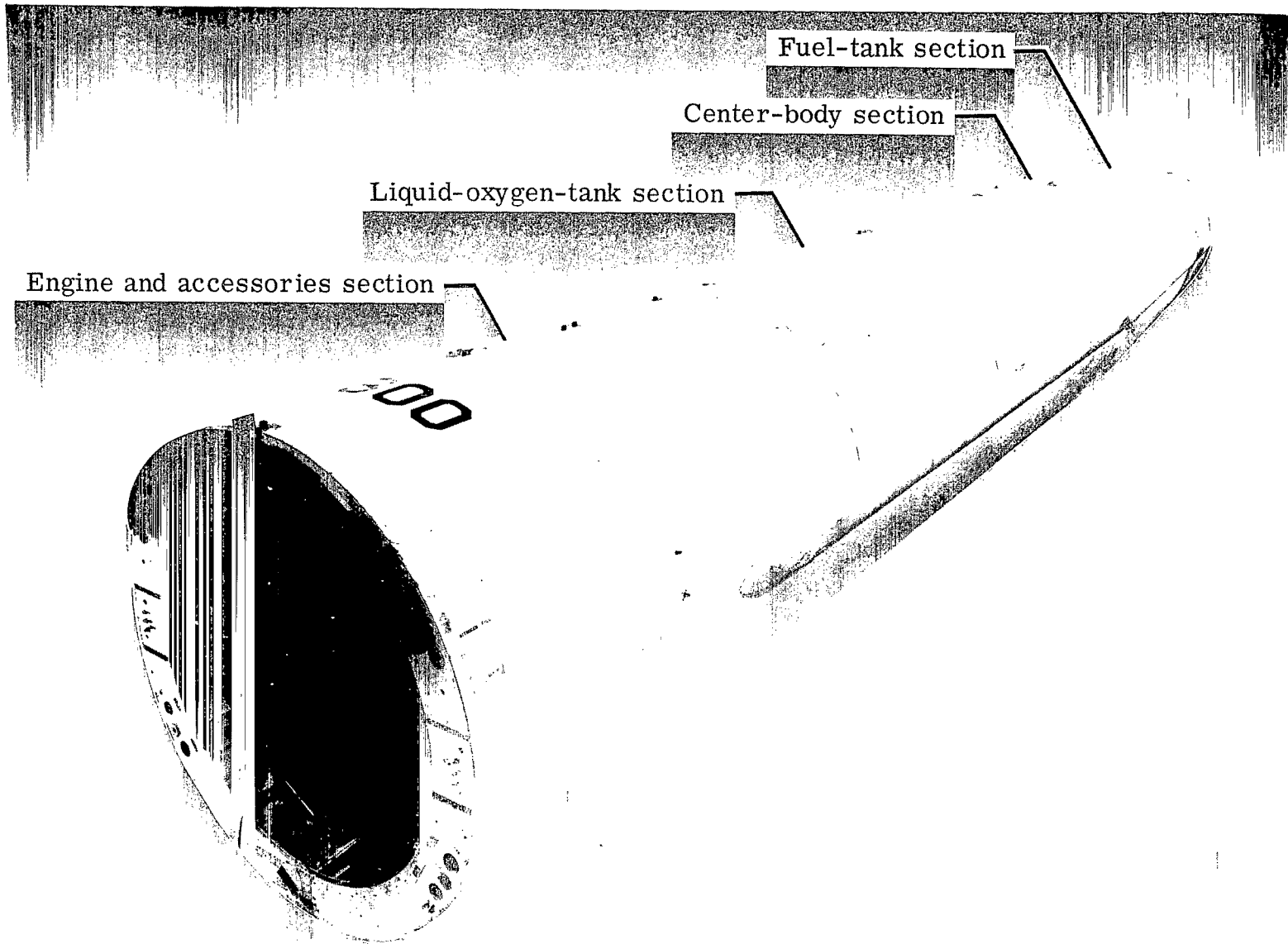


Figure 2.- Assembled test vehicle.

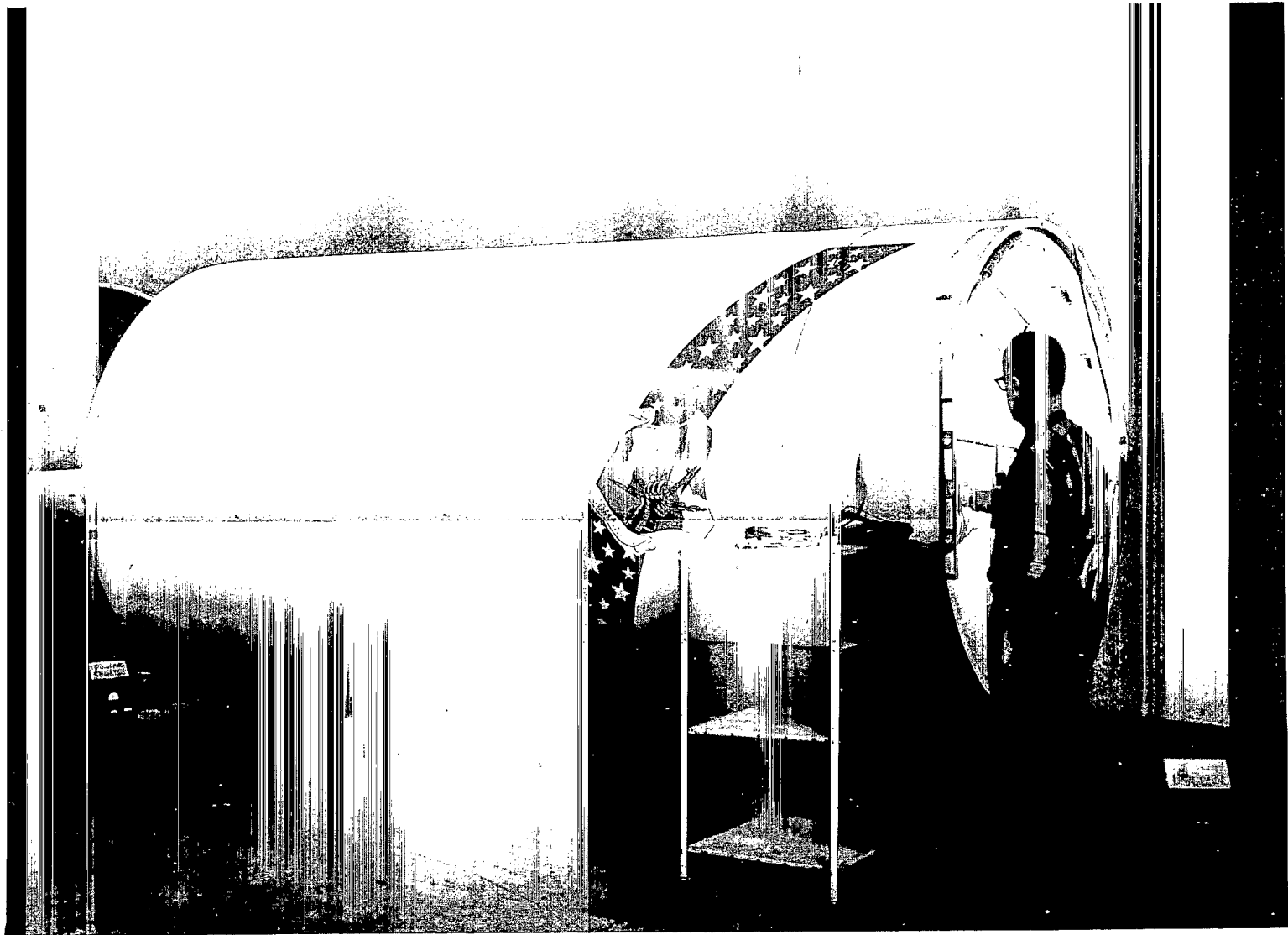


Figure 3.- Fuel-tank section.

L-65-1427.1

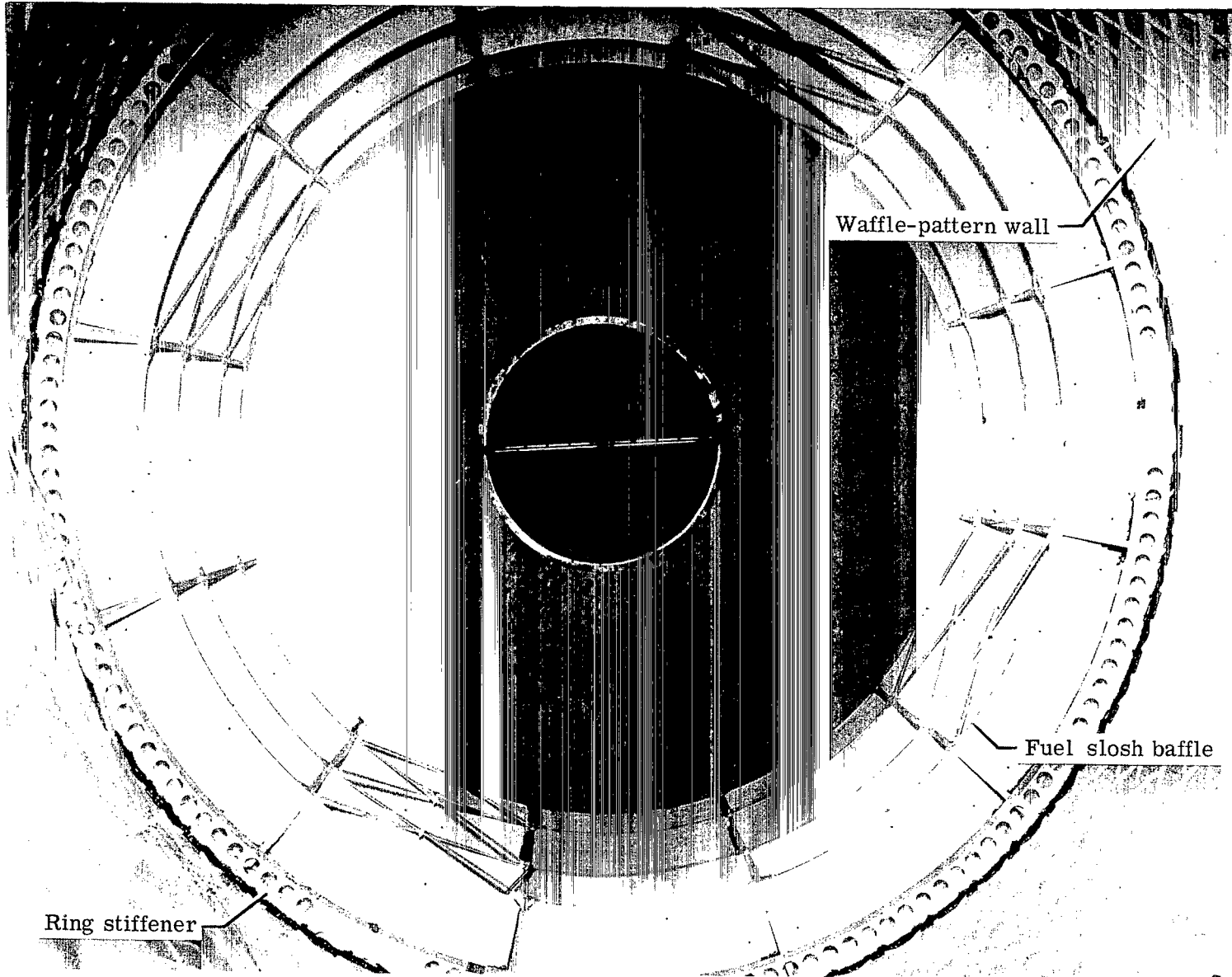


Figure 4.- Interior of fuel tank as viewed looking aft.

L-65-1612.1

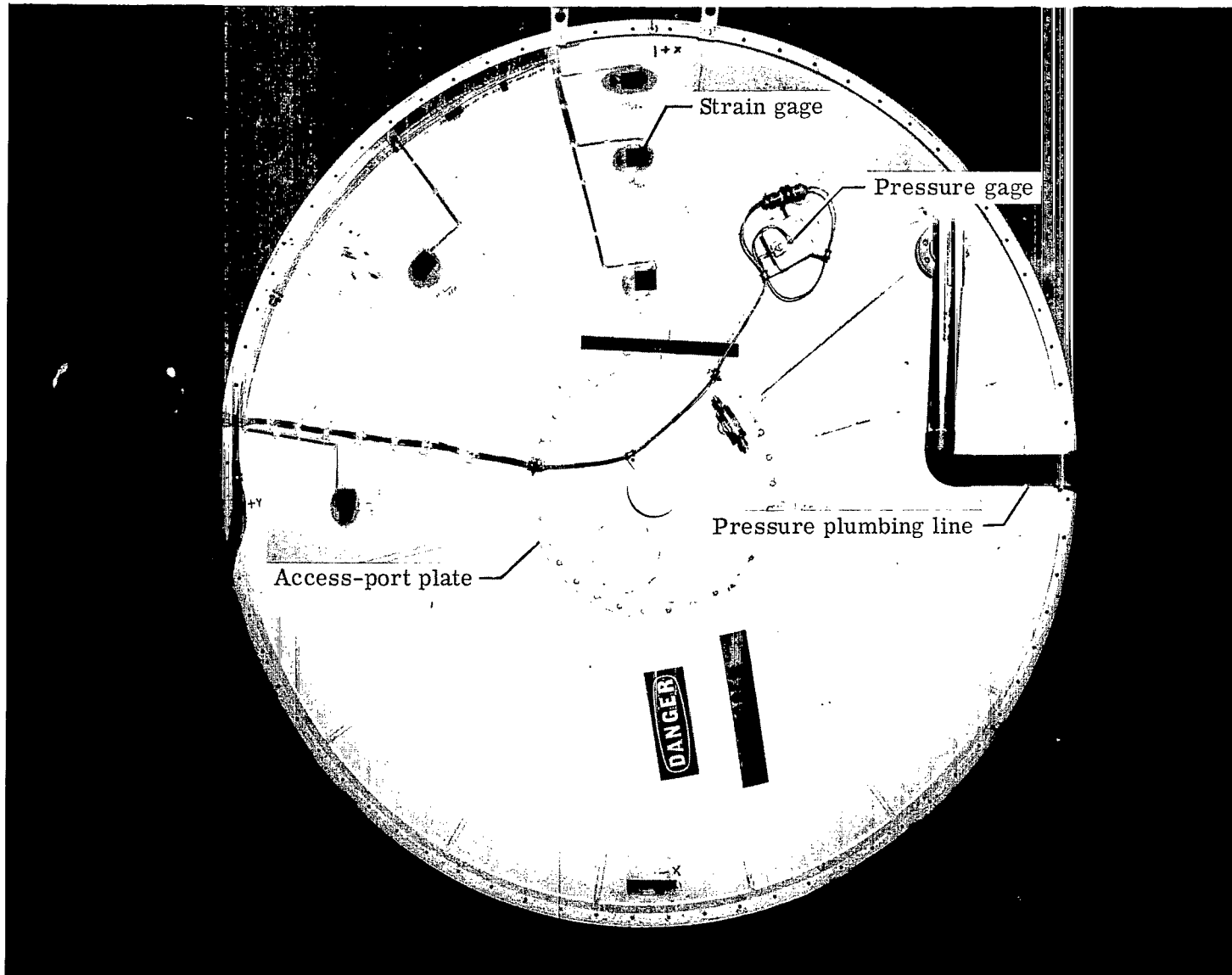


Figure 5.- Forward bulkhead of fuel tank.

L-65-1654.1

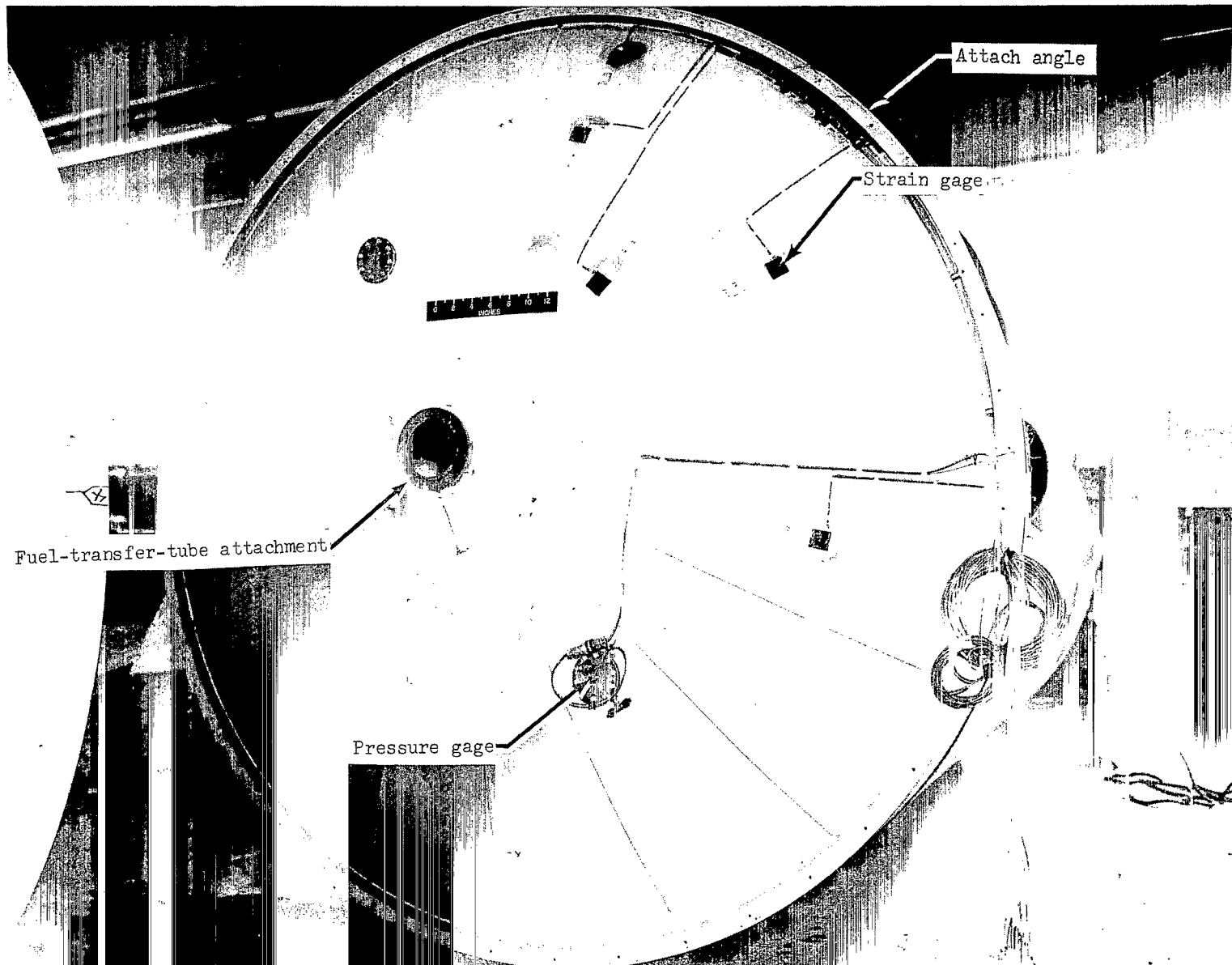


Figure 6.- Aft bulkhead of fuel tank.

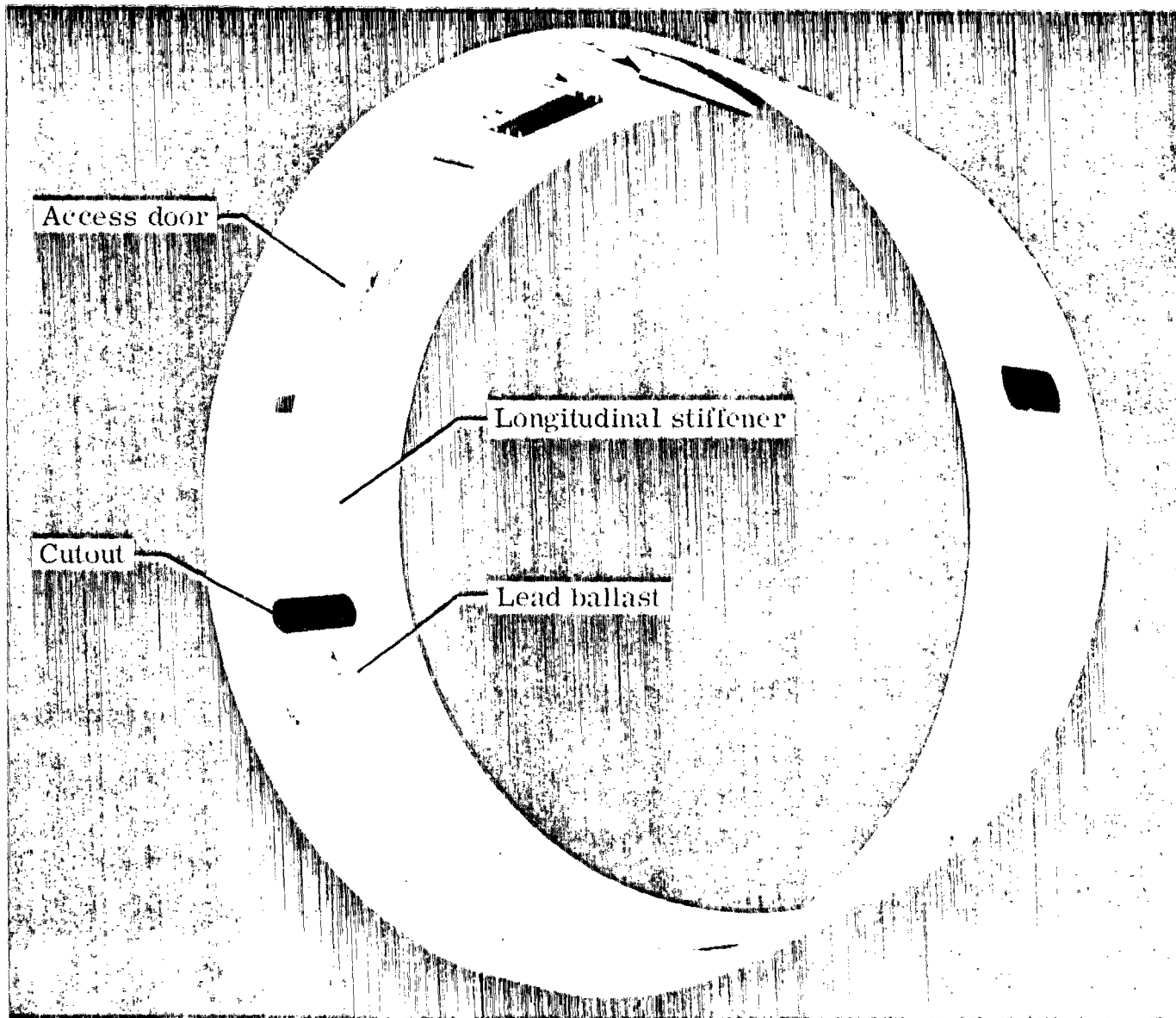


Figure 7.- Center-body section.

1-64-8538.1

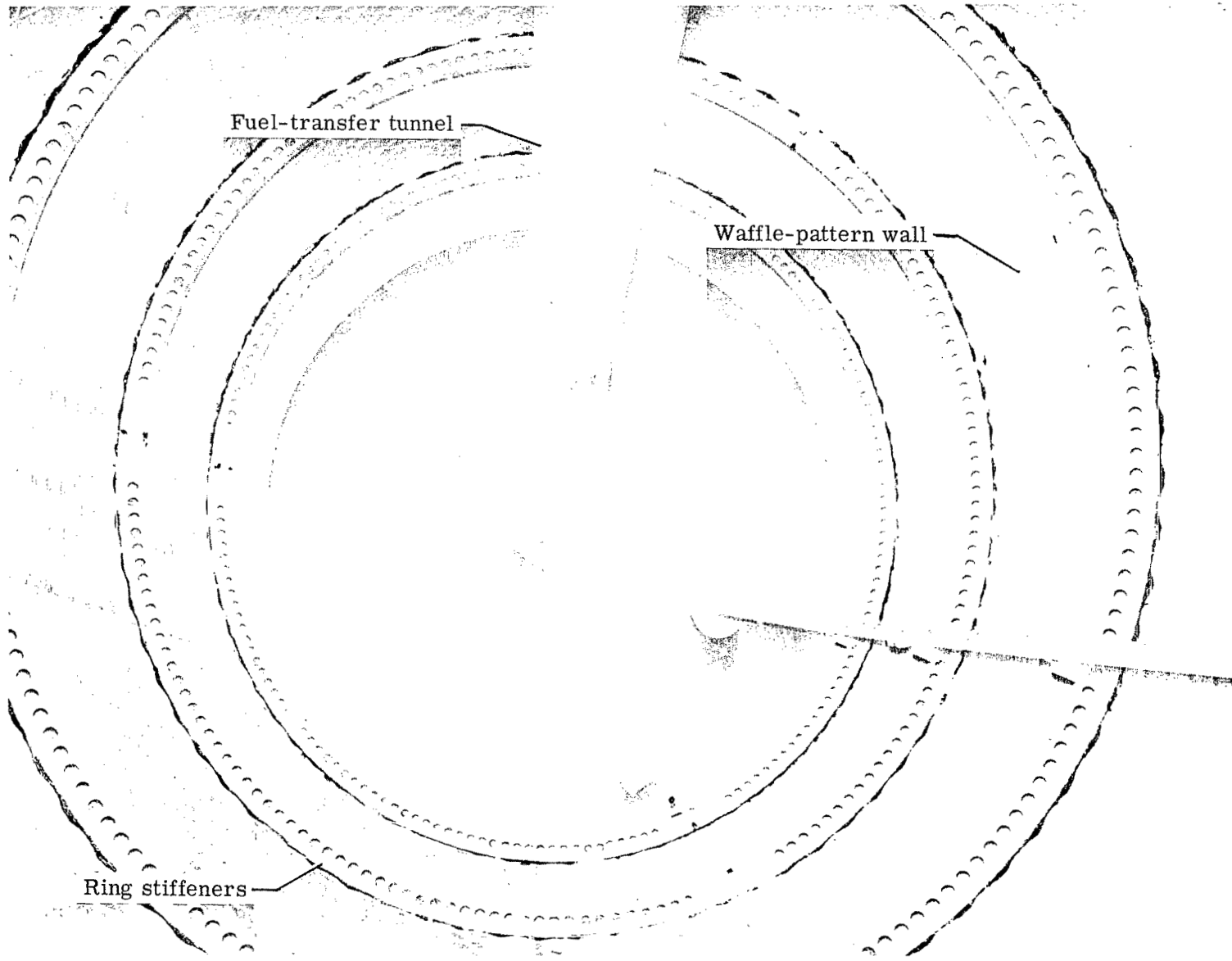


Figure 8.- Interior of liquid-oxygen tank as viewed looking forward.

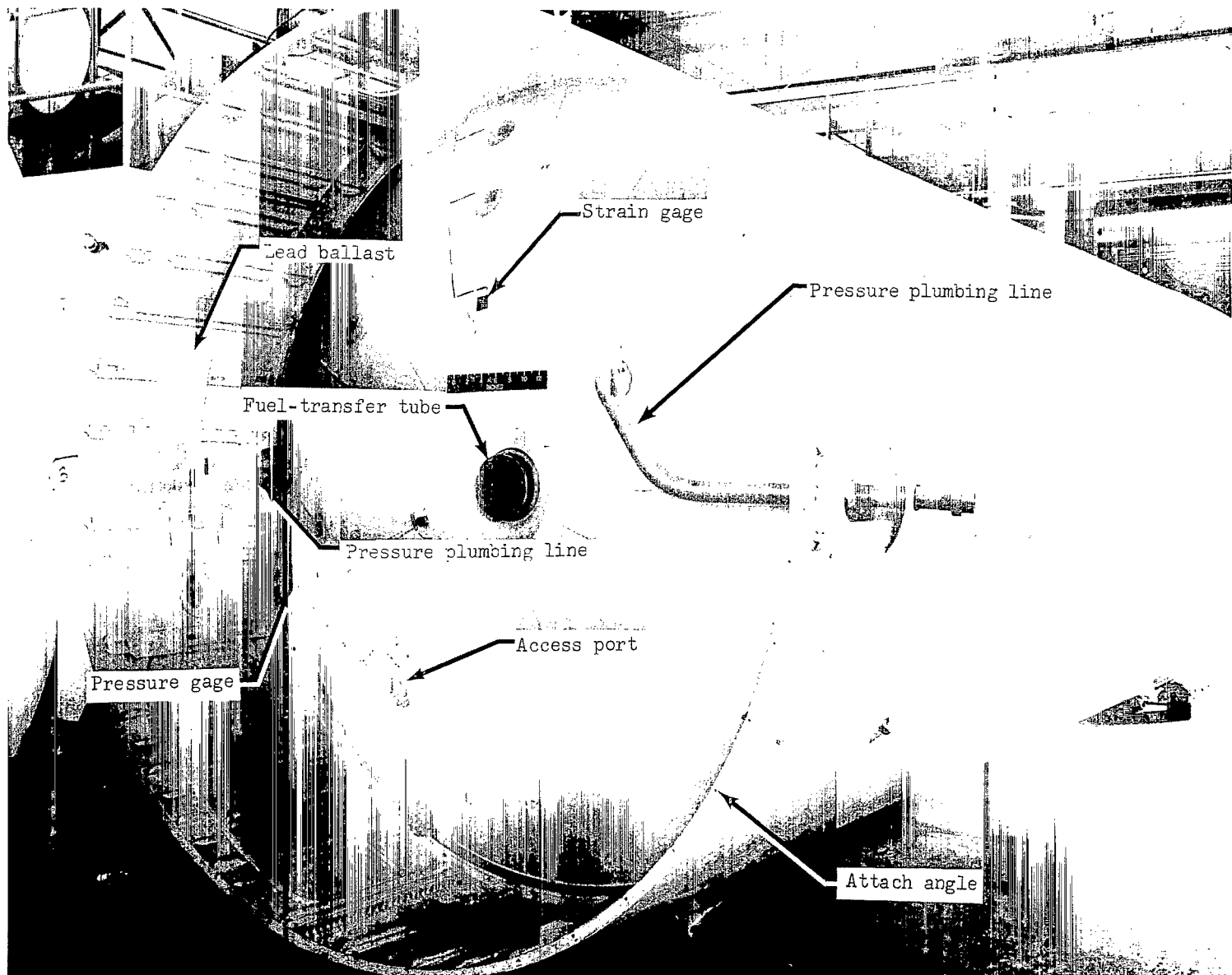


Figure 9.- Forward bulkhead of liquid-oxygen tank and center-body section.

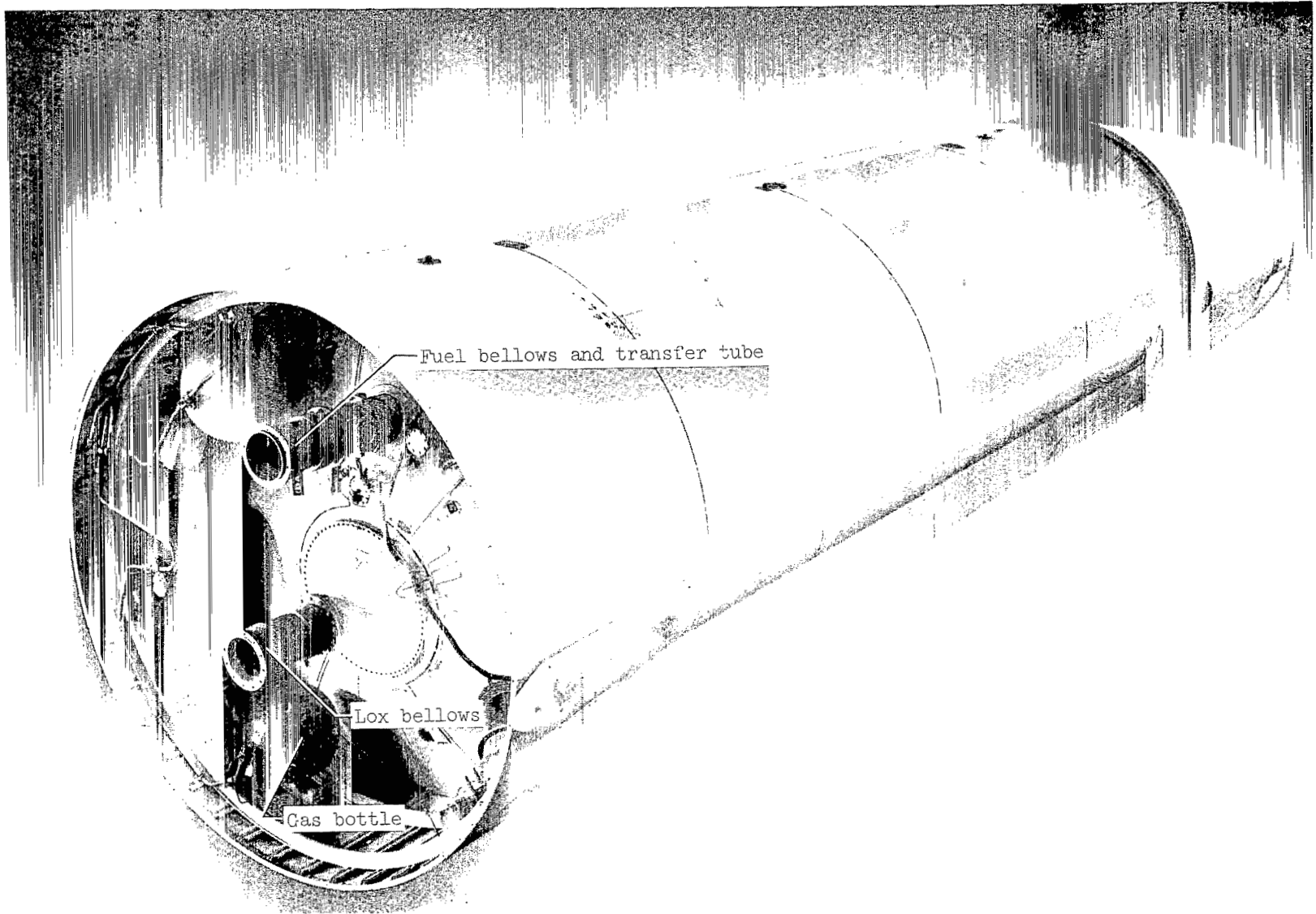


Figure 10.- Aft skirt and aft bulkhead of liquid-oxygen-tank section.

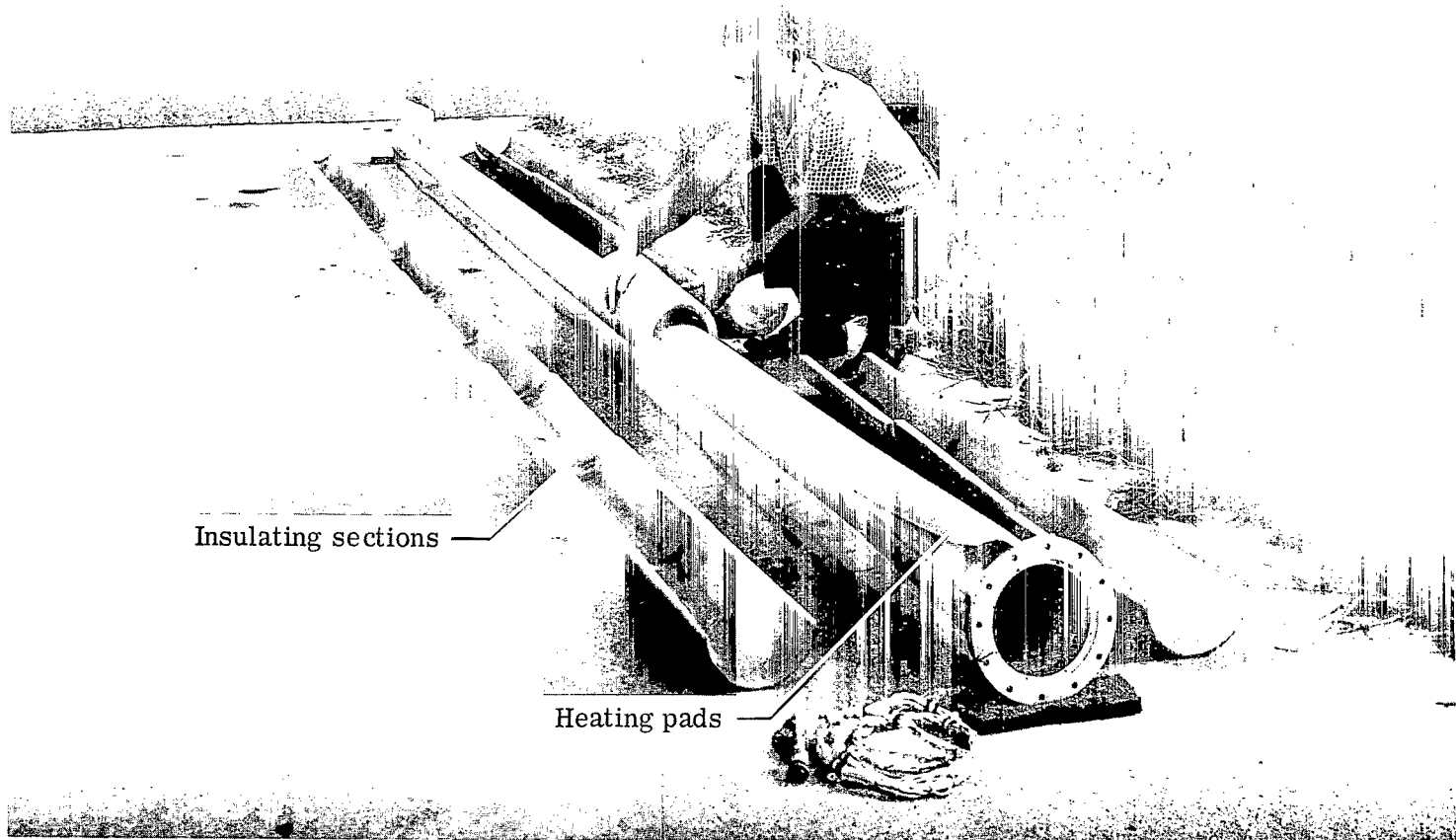


Figure 11.- Fuel-transfer tube and insulating sections (heating pads not included in test vehicle).

L-64-7307.1

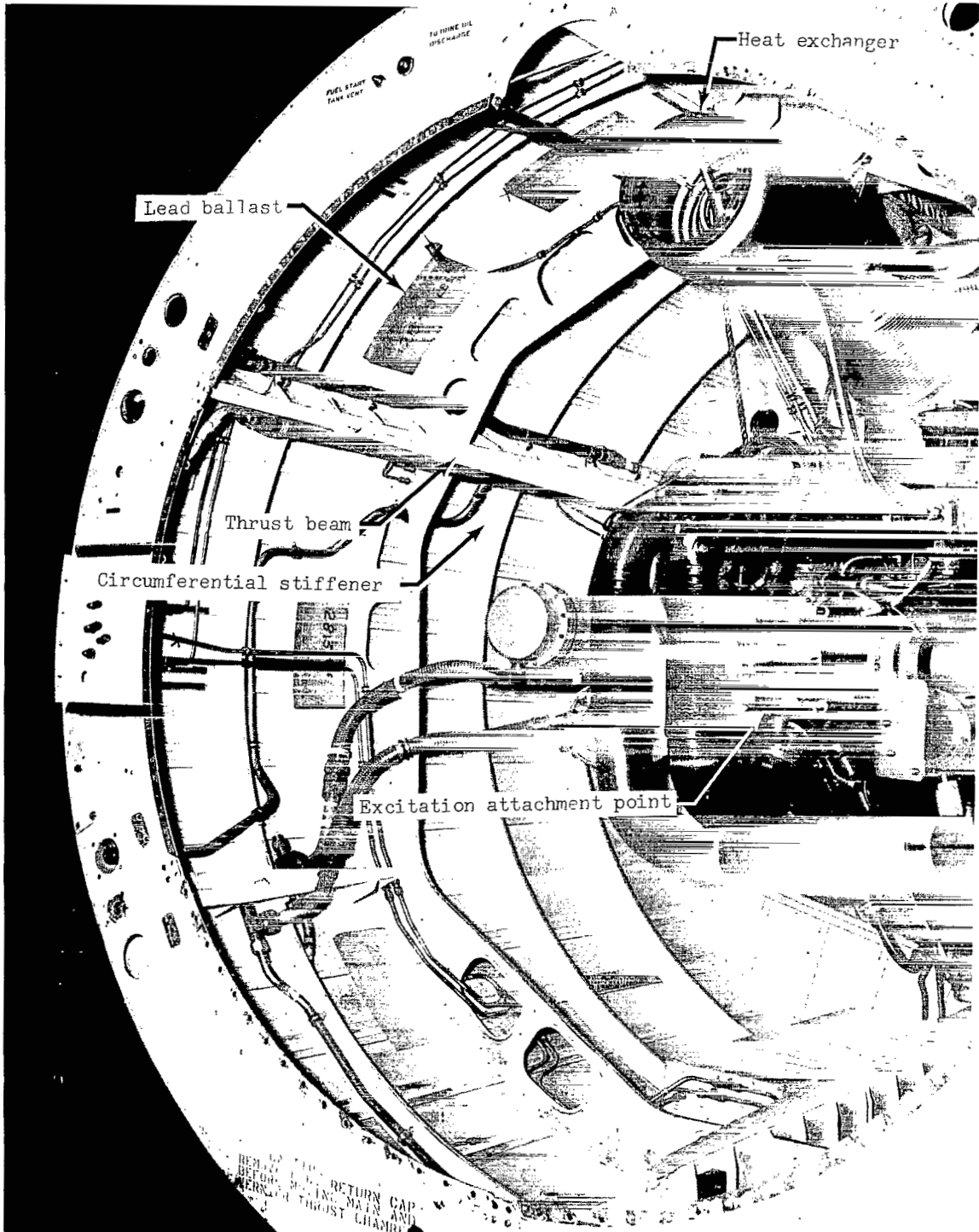


Figure 12.- Engine and accessories section as viewed looking forward at the -Y-axis side of the vehicle.

L-65-1616.1

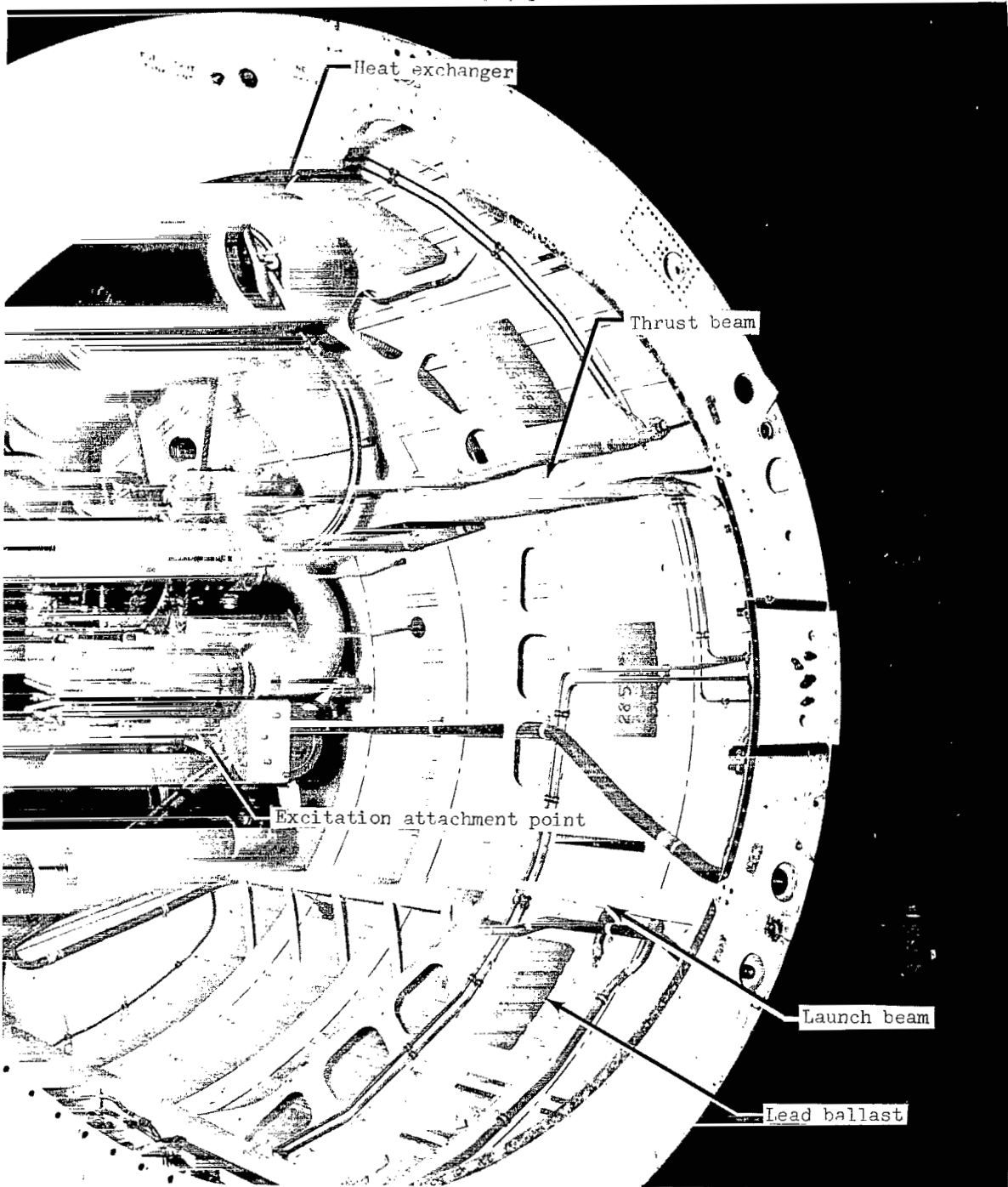


Figure 13.- Engine and accessories section as viewed looking forward at the +Y-axis side of the vehicle.

L-65-1610.1

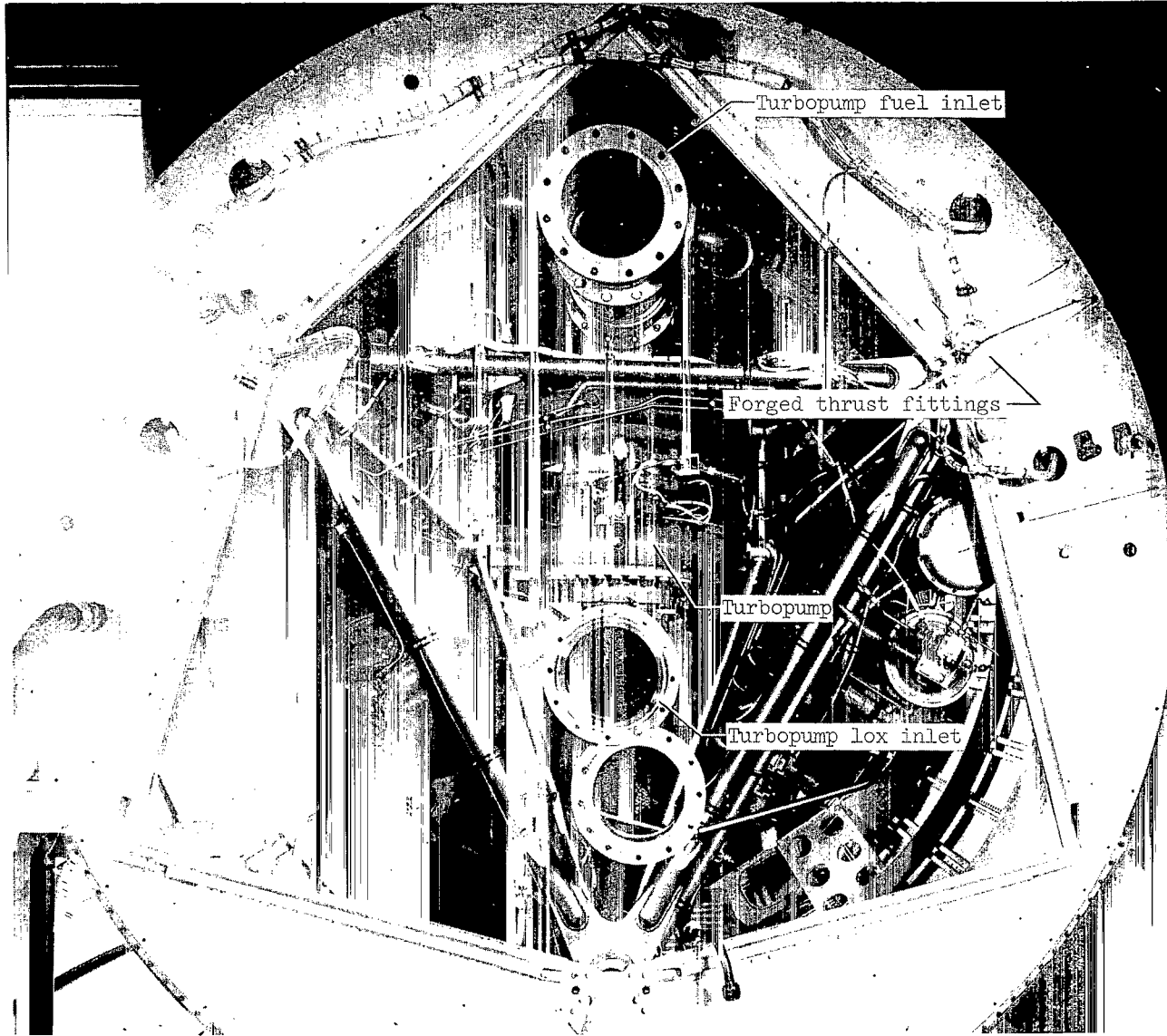


Figure 14.- Engine and accessories section as viewed looking aft.

L-64-6854.1

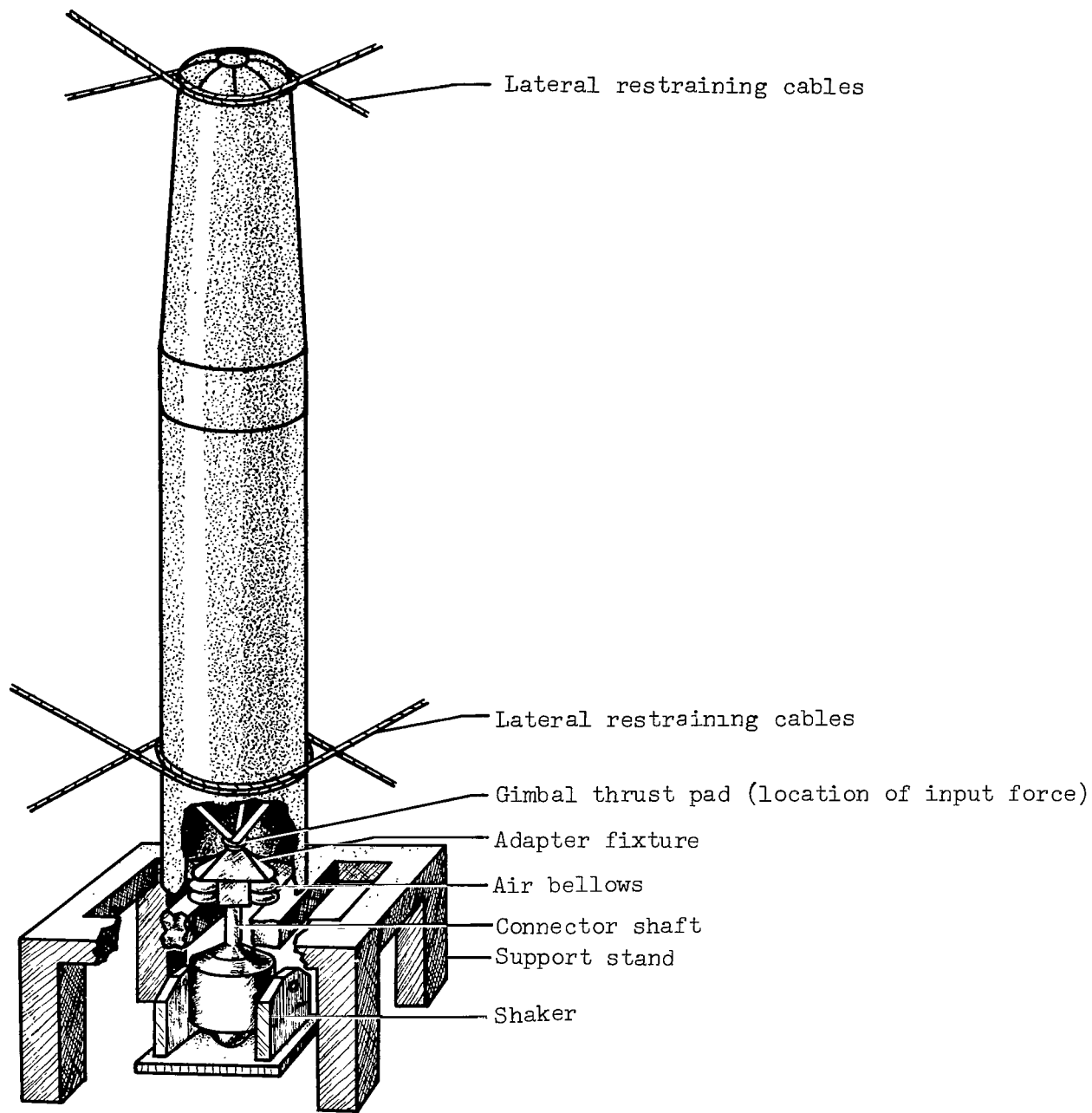
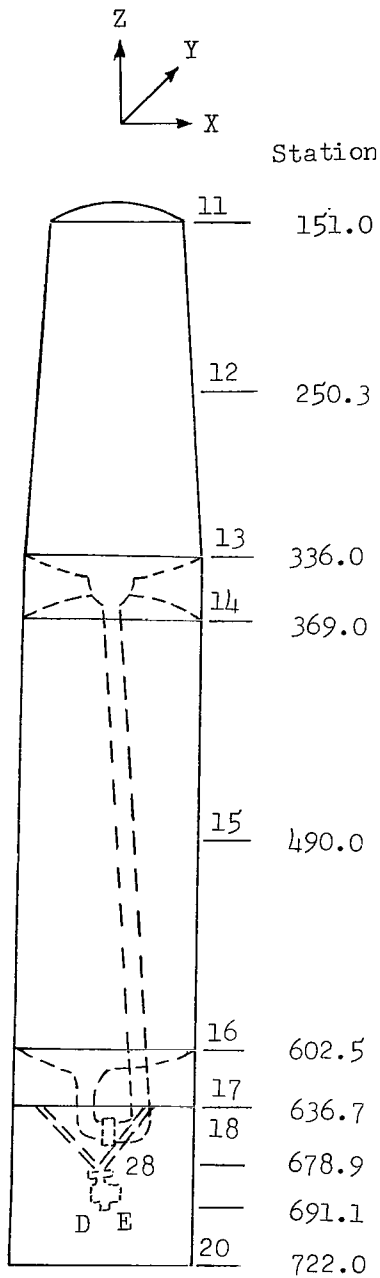


Figure 15.- Longitudinal support system for test vehicle.



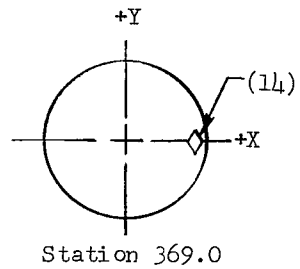
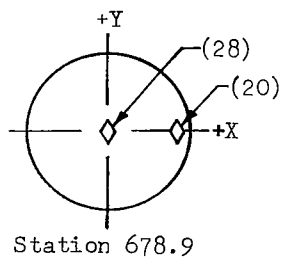
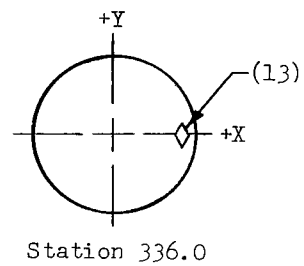
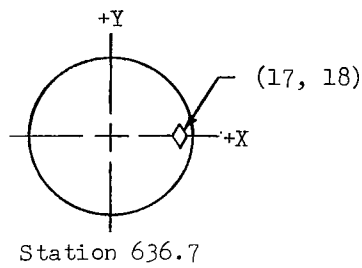
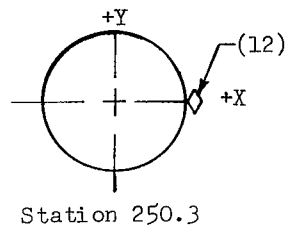
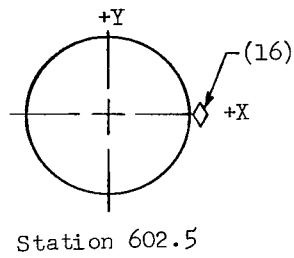
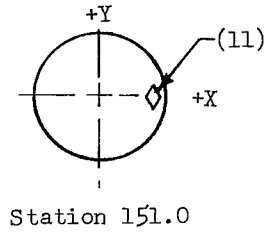
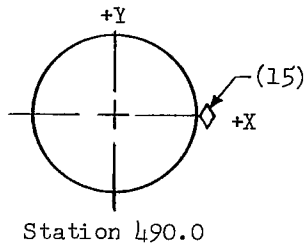
| Accelerometer identification number | Station (Z-axis) | Radial distance, cm | Description |
|-------------------------------------|------------------|---------------------|------------------------|
| 11 | 151.0 | 92.7 | Attach angle |
| 12 | 250.3 | 109.5 | Skin |
| 13 | 336.0 | 119.4 | Attach angle |
| 14 | 369.0 | 119.4 | Attach angle |
| 15 | 490.0 | 121.9 | Skin |
| 16 | 602.5 | 121.9 | Skin |
| 17 | 636.4 | 119.4 | Attach angle |
| 18 | 637.0 | 119.4 | Attach angle |
| 20 | 720.0 | 119.4 | Aft end of vehicle |
| 28 | 678.9 | 0 | Bottom of thrust frame |
| D | 691.1 | 0 | Input force |
| E | 691.1 | 10.2 | Input accelerometer |

(a) Longitudinal and radial locations.

Figure 16. Accelerometer locations on the test vehicle. Data group 1.

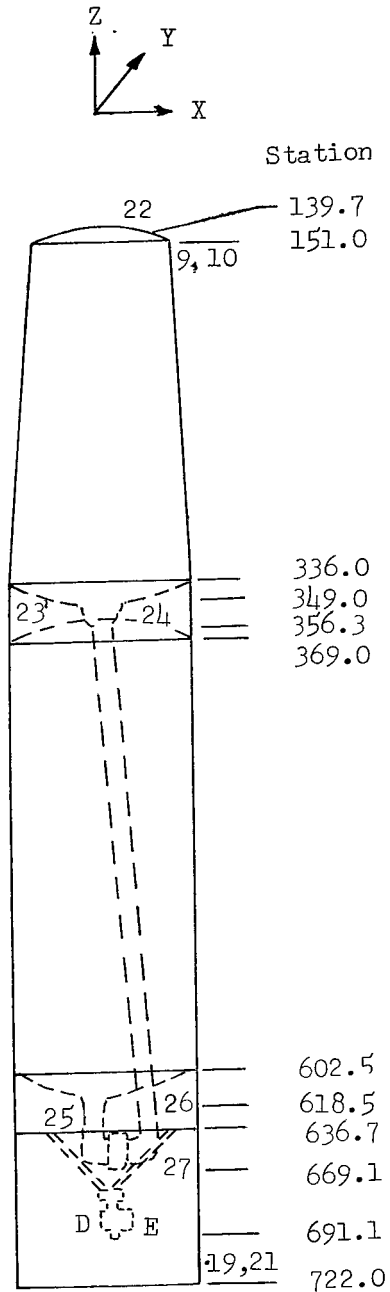
Accelerometer
orientation

◇ +Z



(b) Radial location, looking aft, of accelerometers.

Figure 16.- Concluded.



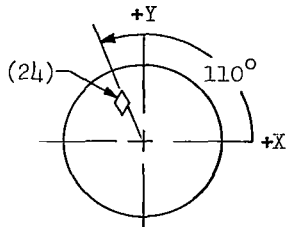
| Accelerometer identification number | Station (Z-axis) | Radial distance, cm | Description |
|-------------------------------------|------------------|---------------------|------------------------------|
| 9 | 151.0 | 92.7 | Attach angle |
| 10 | 151.0 | 92.7 | Attach angle |
| 19 | 720.0 | 119.4 | Attach angle |
| 21 | 720.0 | 119.4 | Attach angle |
| 22 | 139.7 | 53.3 | Top bulkhead of fuel tank |
| 23 | 347.0 | 55.9 | Bottom bulkhead of fuel tank |
| 24 | 356.3 | 81.3 | Top bulkhead of lox tank |
| 25 | 618.9 | 28.4 | Bottom bulkhead of lox tank |
| 26 | 618.5 | 73.7 | Fuel transfer flange |
| 27 | 669.1 | 20.3 | Pump |
| D | 691.1 | 0.0 | Input force |
| E | 691.1 | 10.2 | Input accelerometer |

(a) Longitudinal and radial locations.

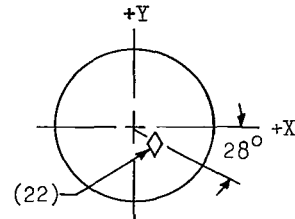
Figure 17.- Accelerometer locations on the test vehicle. Data group 2.

Accelerometer
orientation

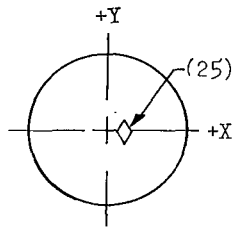
- ◇ +Z
- +X
- △ +Y



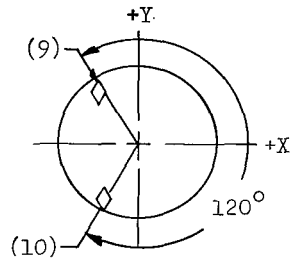
Top lox-tank bulkhead



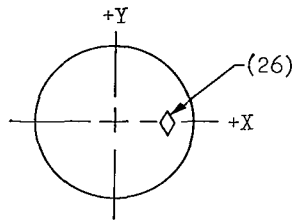
Top fuel-tank bulkhead



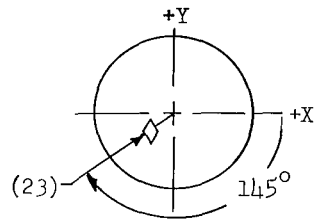
Bottom lox-tank bulkhead



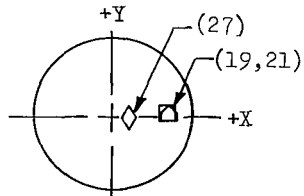
Station 151.0



Fuel transfer flange



Bottom fuel-tank bulkhead



Station 722.0

(b) Radial location, looking aft, of accelerometers.

Figure 17.- Concluded.

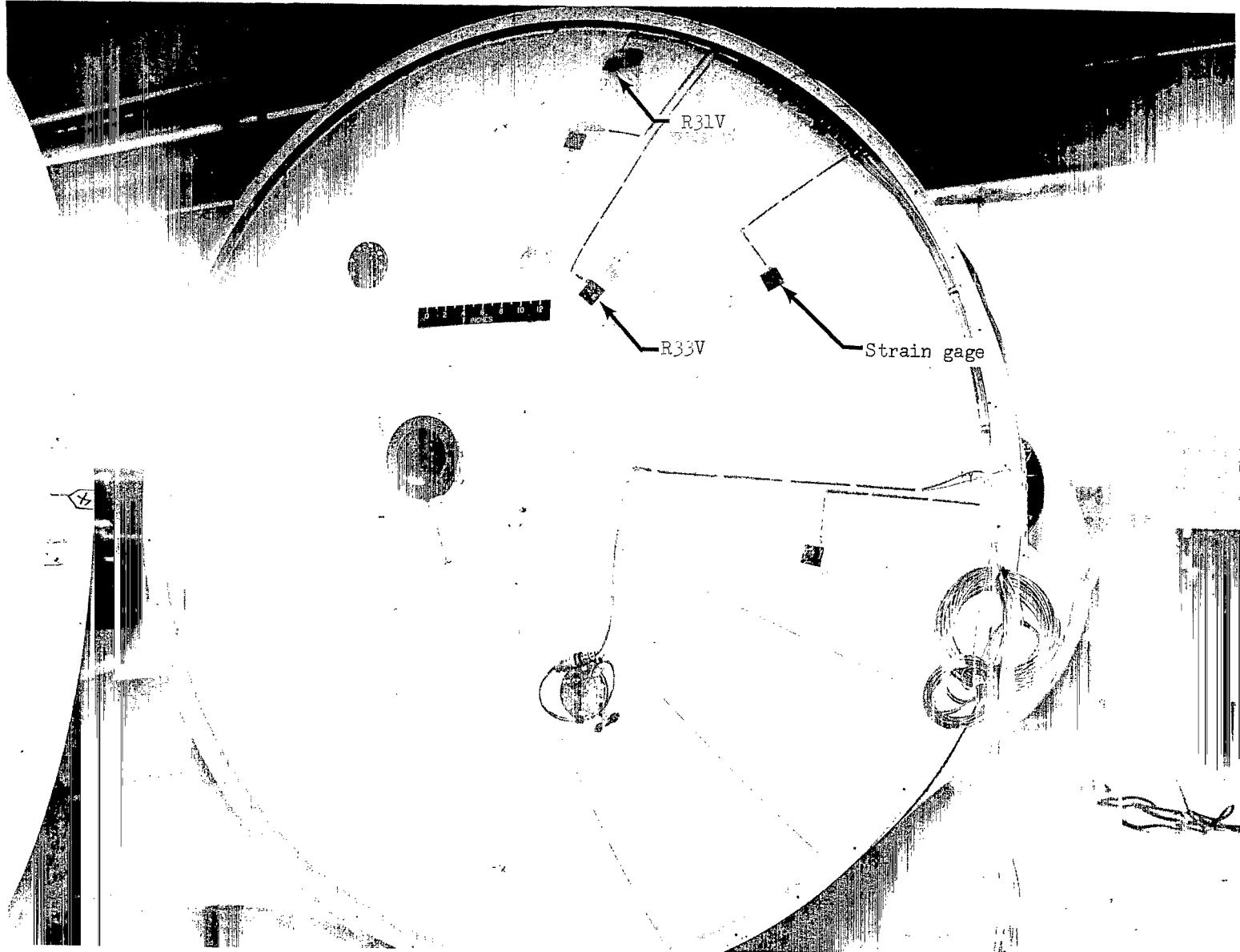


Figure 18.- Strain-gage locations on the bottom bulkhead of the fuel tank.

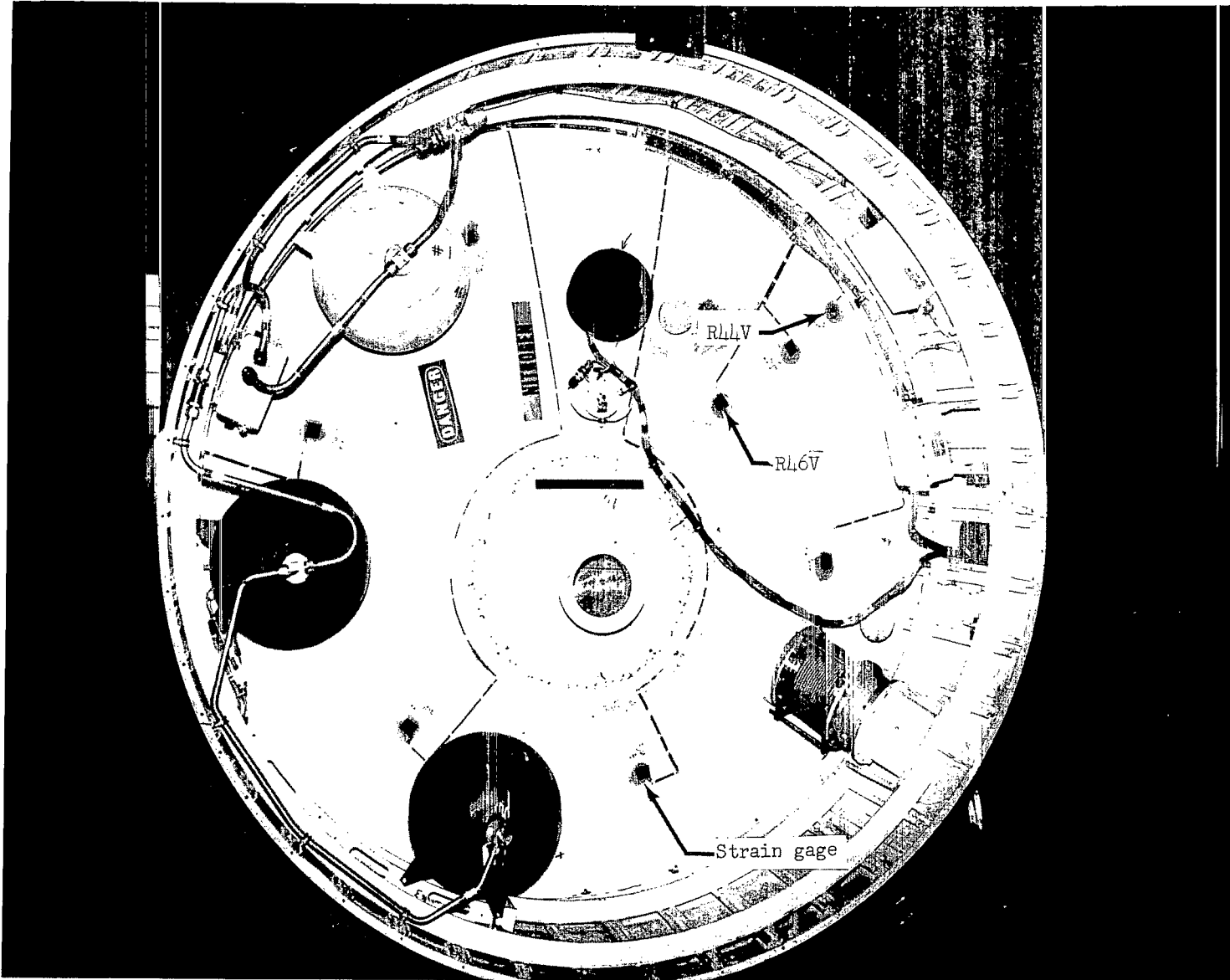


Figure 19.- Strain-gage locations on the bottom bulkhead of the liquid-oxygen tank.

L-65-1652.1

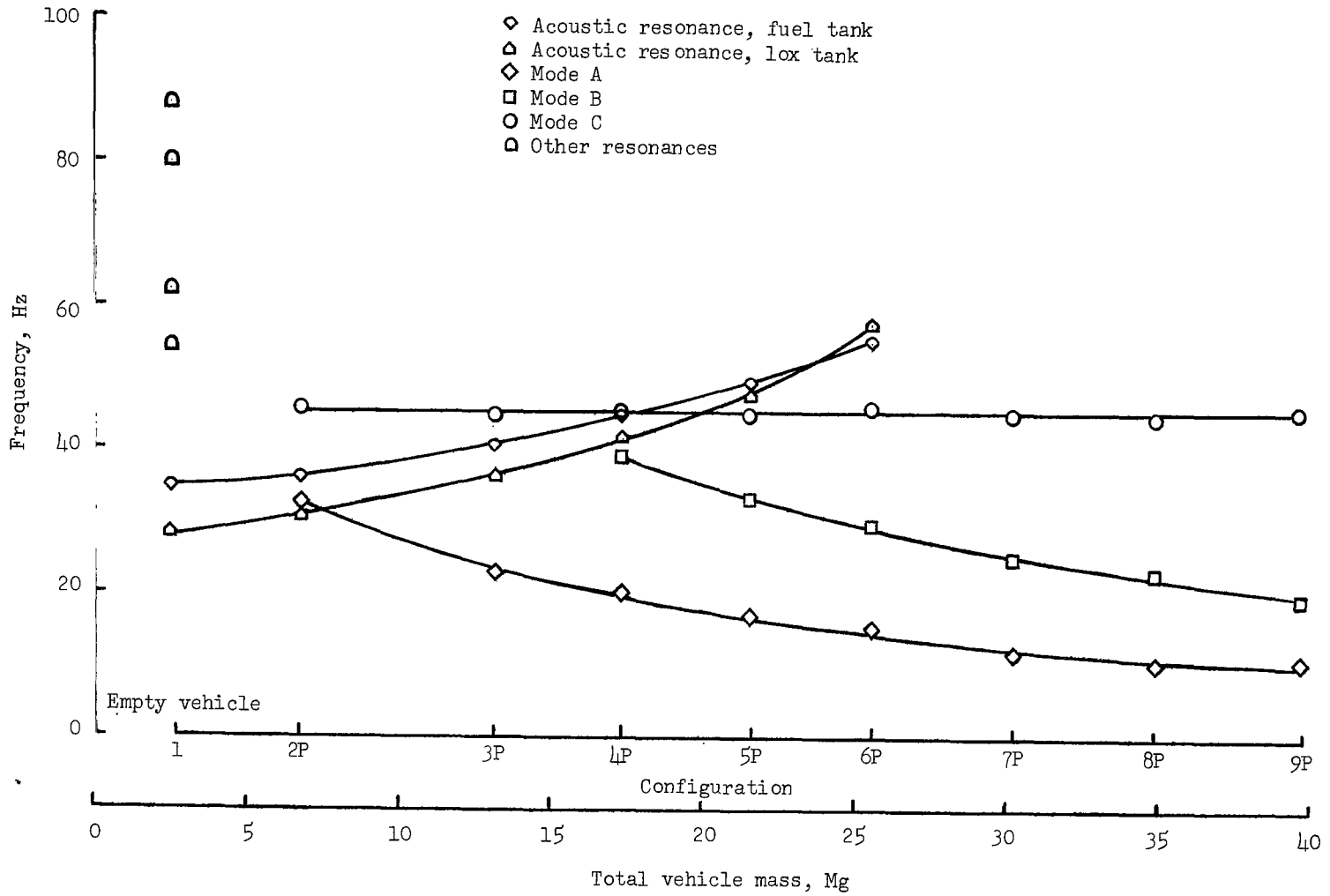
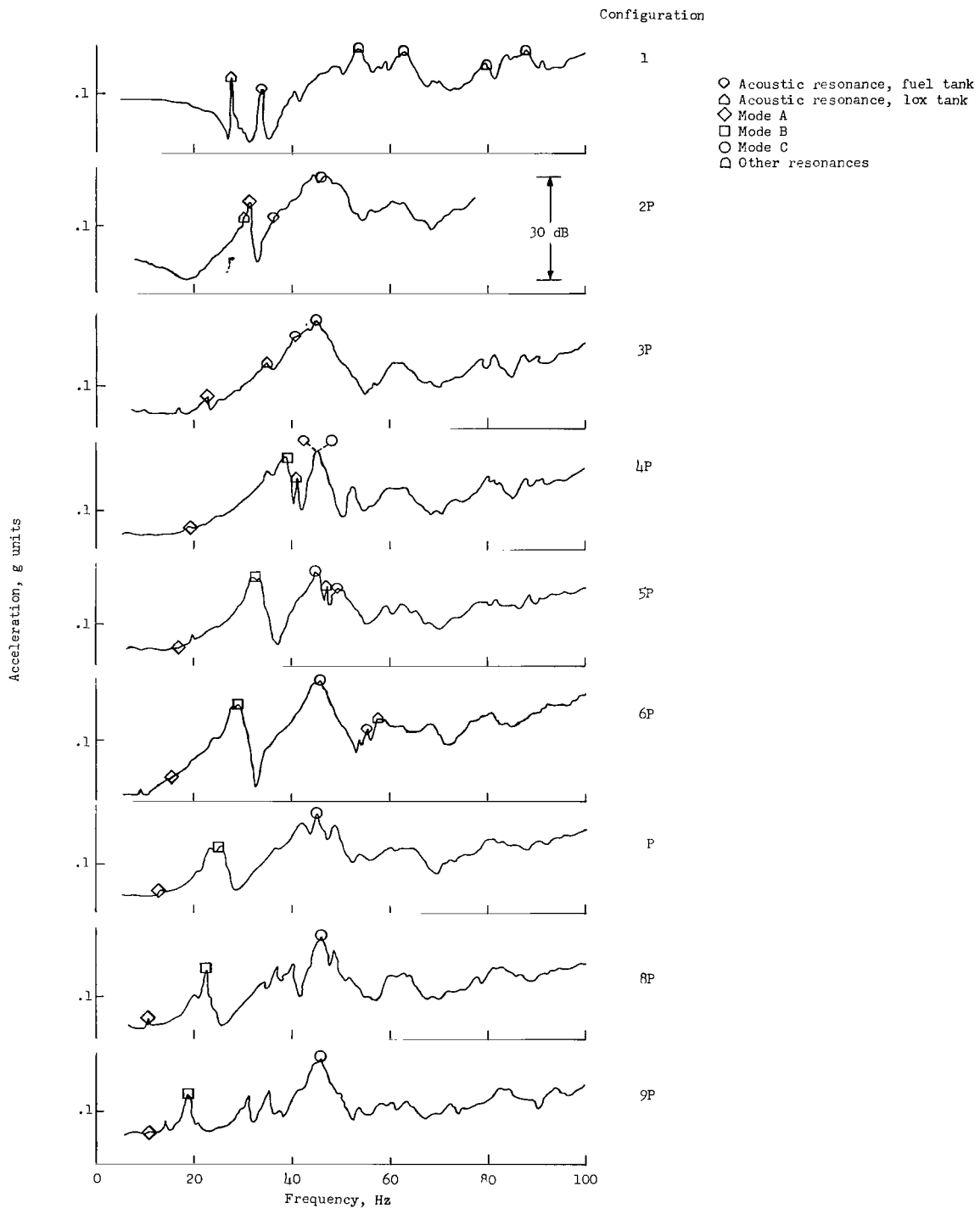
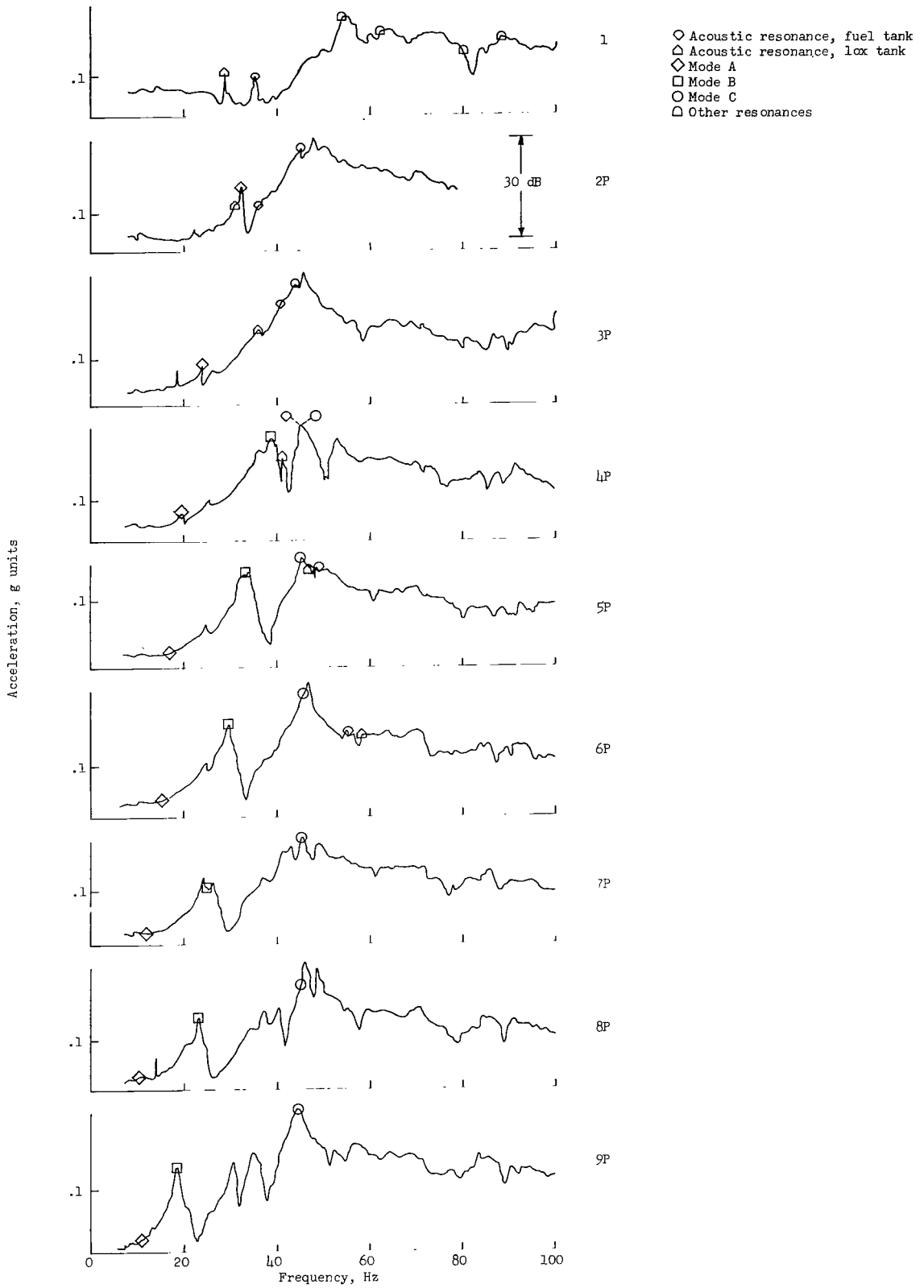


Figure 20.- Variation of frequency with vehicle mass.

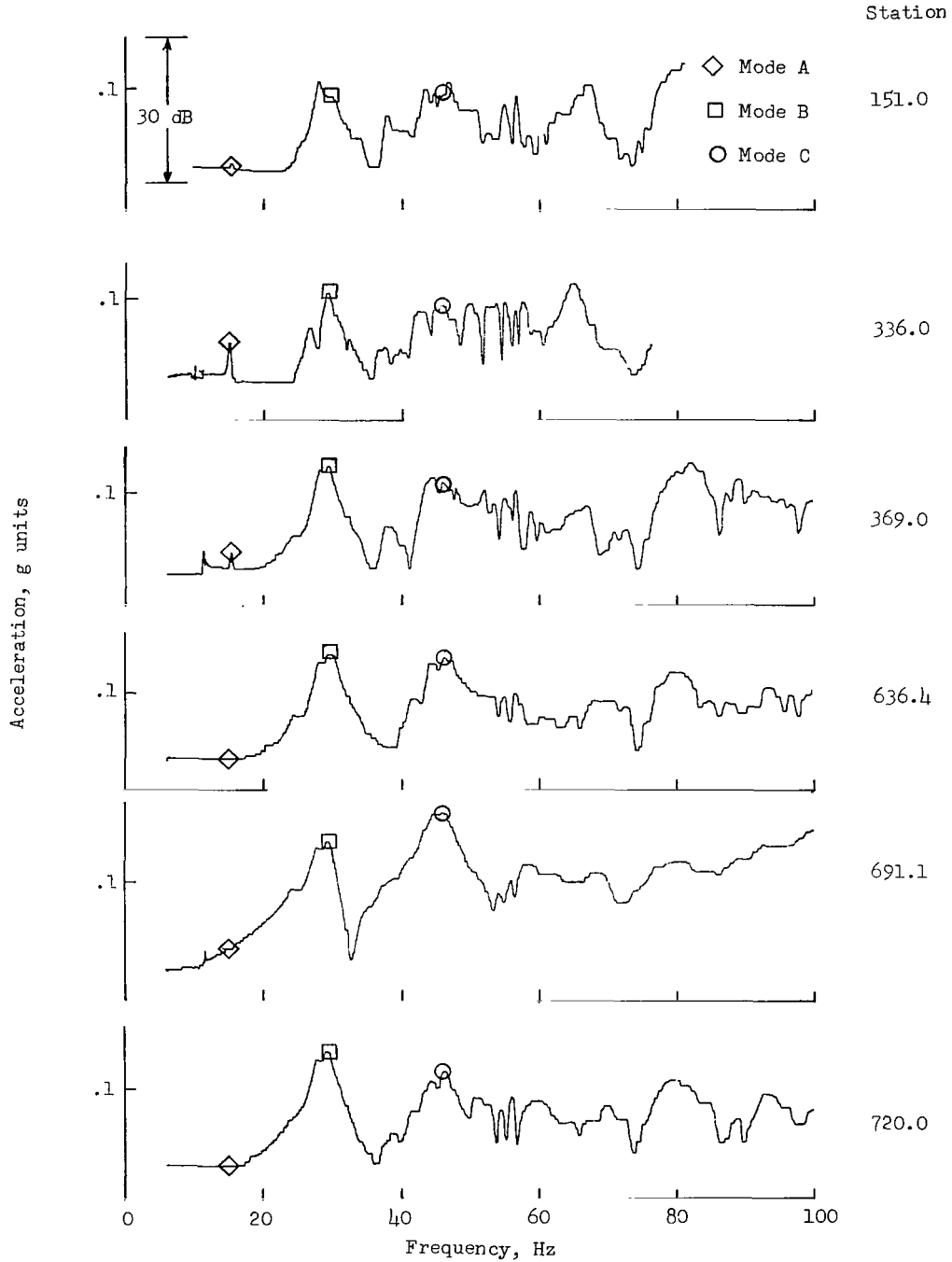


(a) Acceleration measured at station 691.1 (location of input force).

Figure 21.- Frequency response of various vehicle configurations when excited by a constant force of ± 1334 newtons.

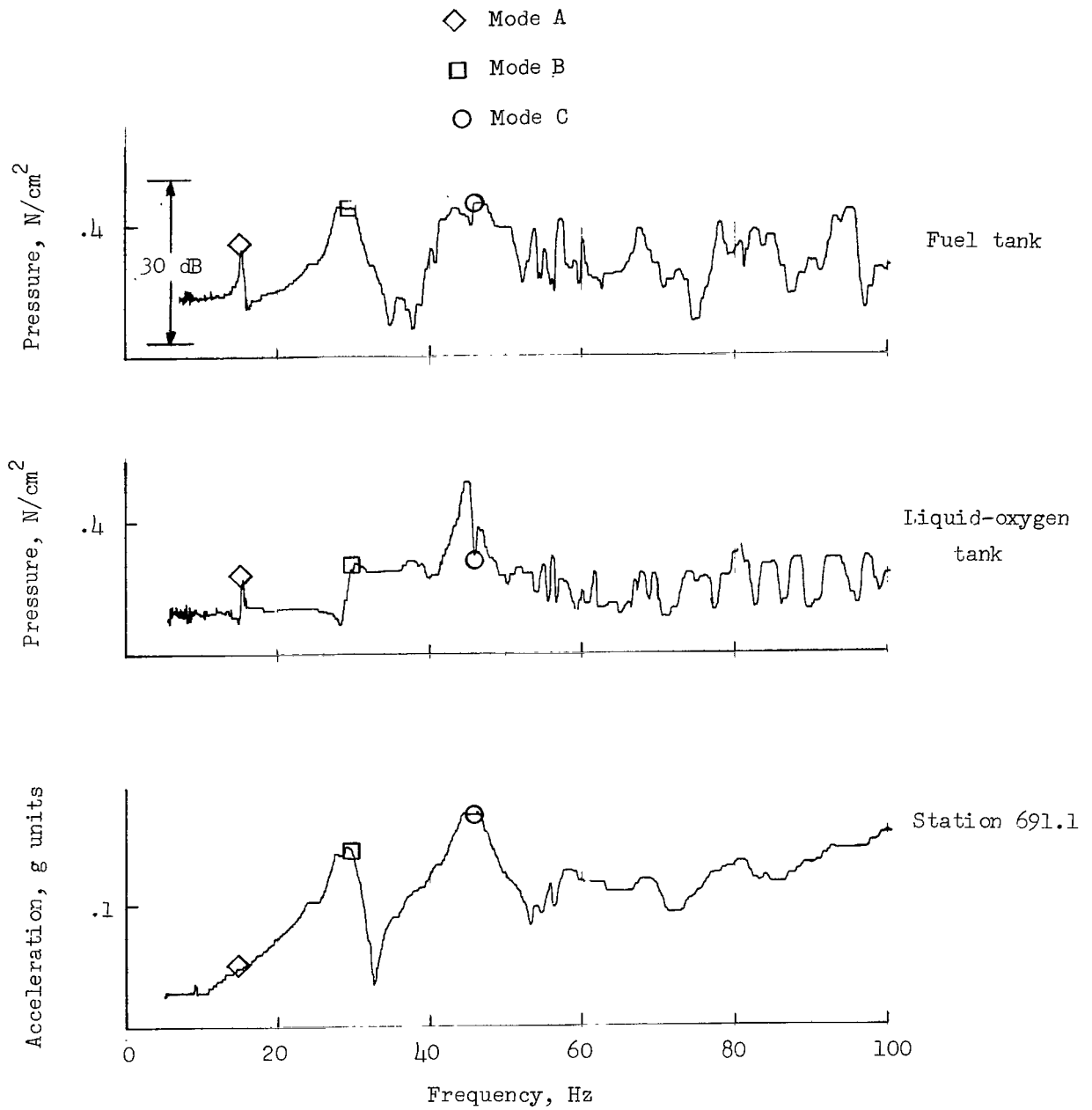


(b) Acceleration measured on the turbopump.



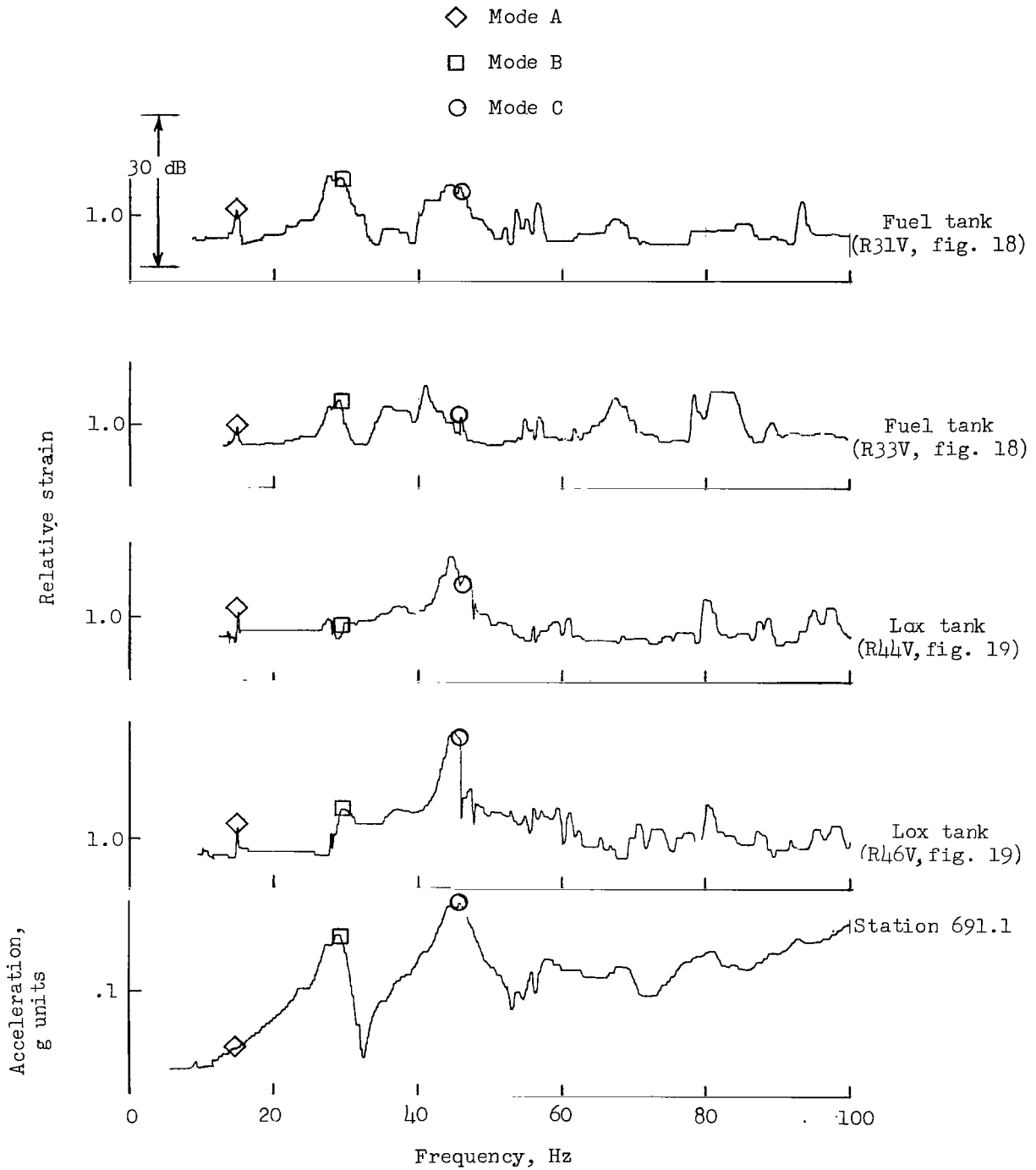
(a) Acceleration measured at various stations.

Figure 22.- Frequency response of vehicle configuration 6P when excited by a constant force. (Acceleration at station 691.1 shown for reference.)



(b) Pressure measured on bottom bulkheads of fuel and liquid-oxygen tanks.

Figure 22.- Continued.



(c) Relative strains measured on bottom bulkheads of fuel and liquid-oxygen tanks.

Figure 22.- Concluded.

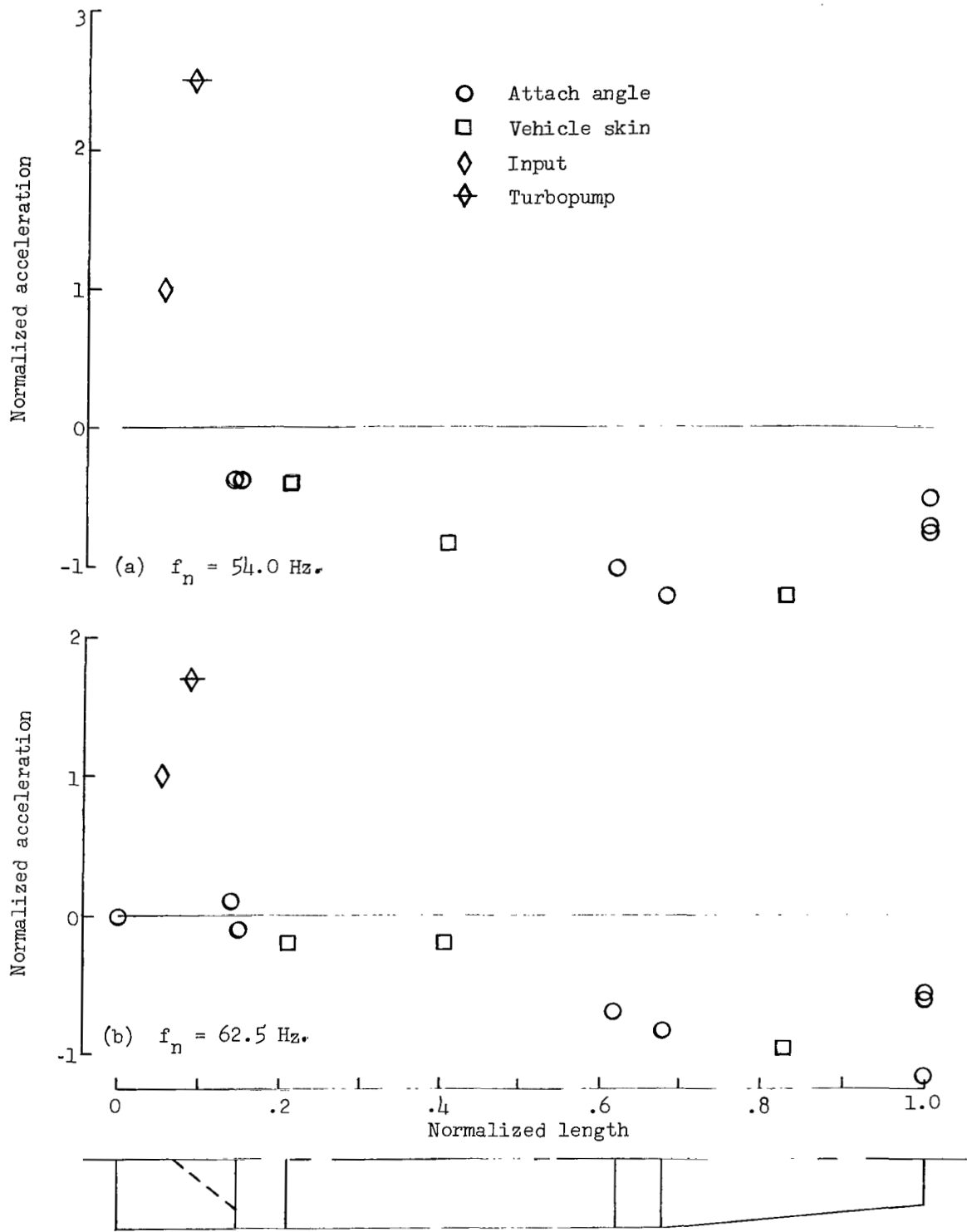


Figure 23.- Resonant response accelerations for vehicle configuration 1.

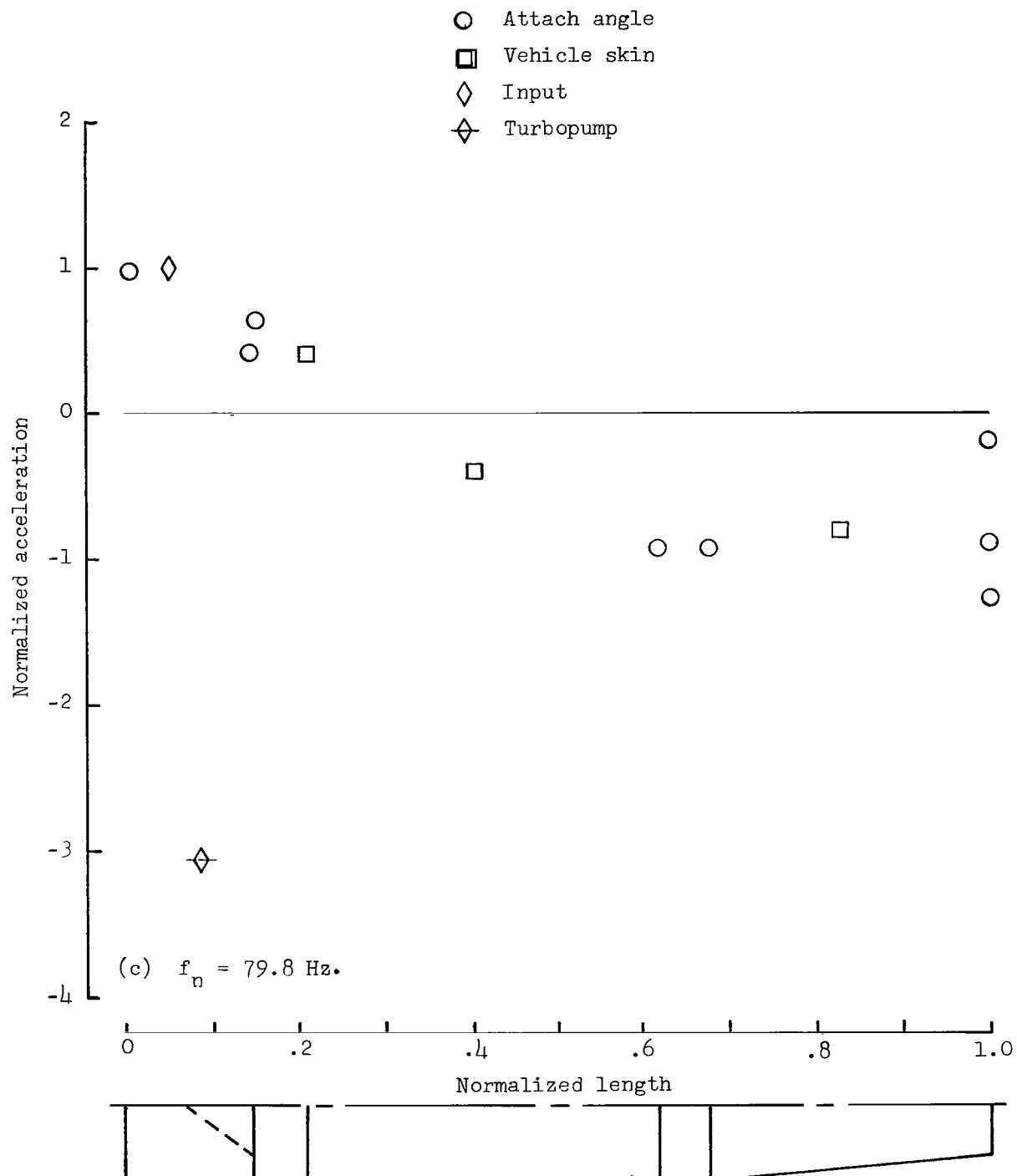


Figure 23.- Continued.

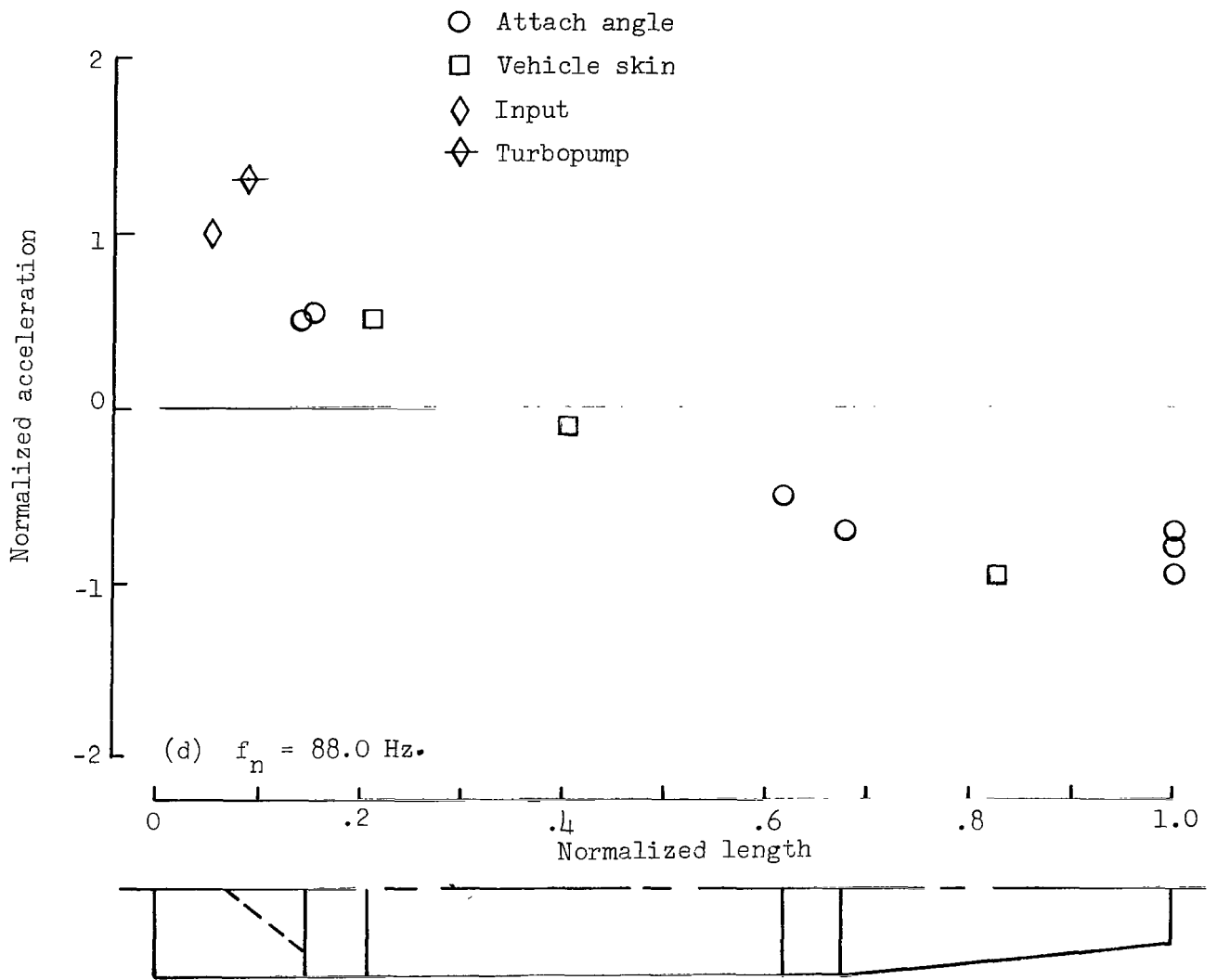


Figure 23.- Concluded.

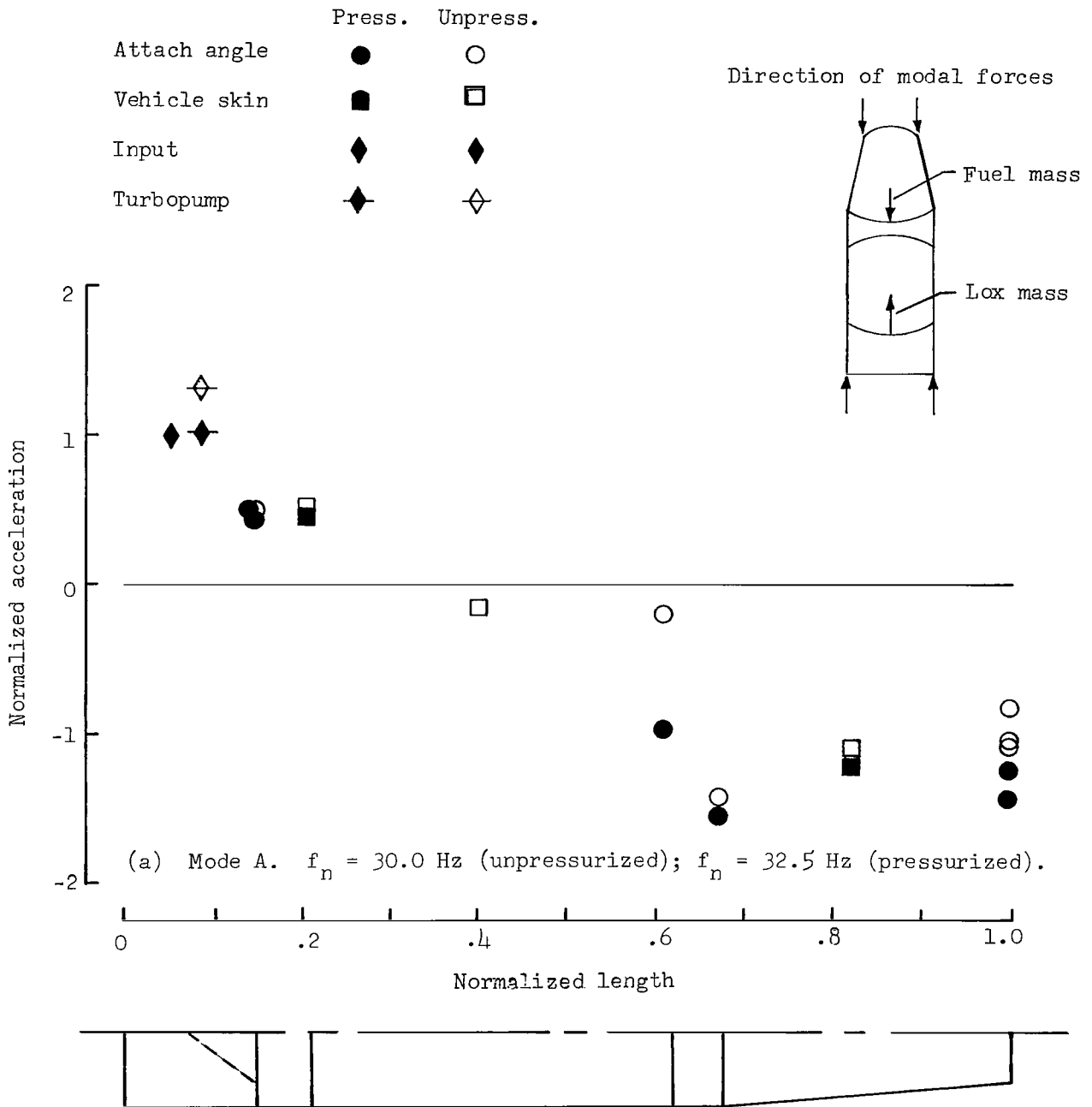


Figure 24.- Resonant response accelerations of vehicle configurations 2 and 2P.

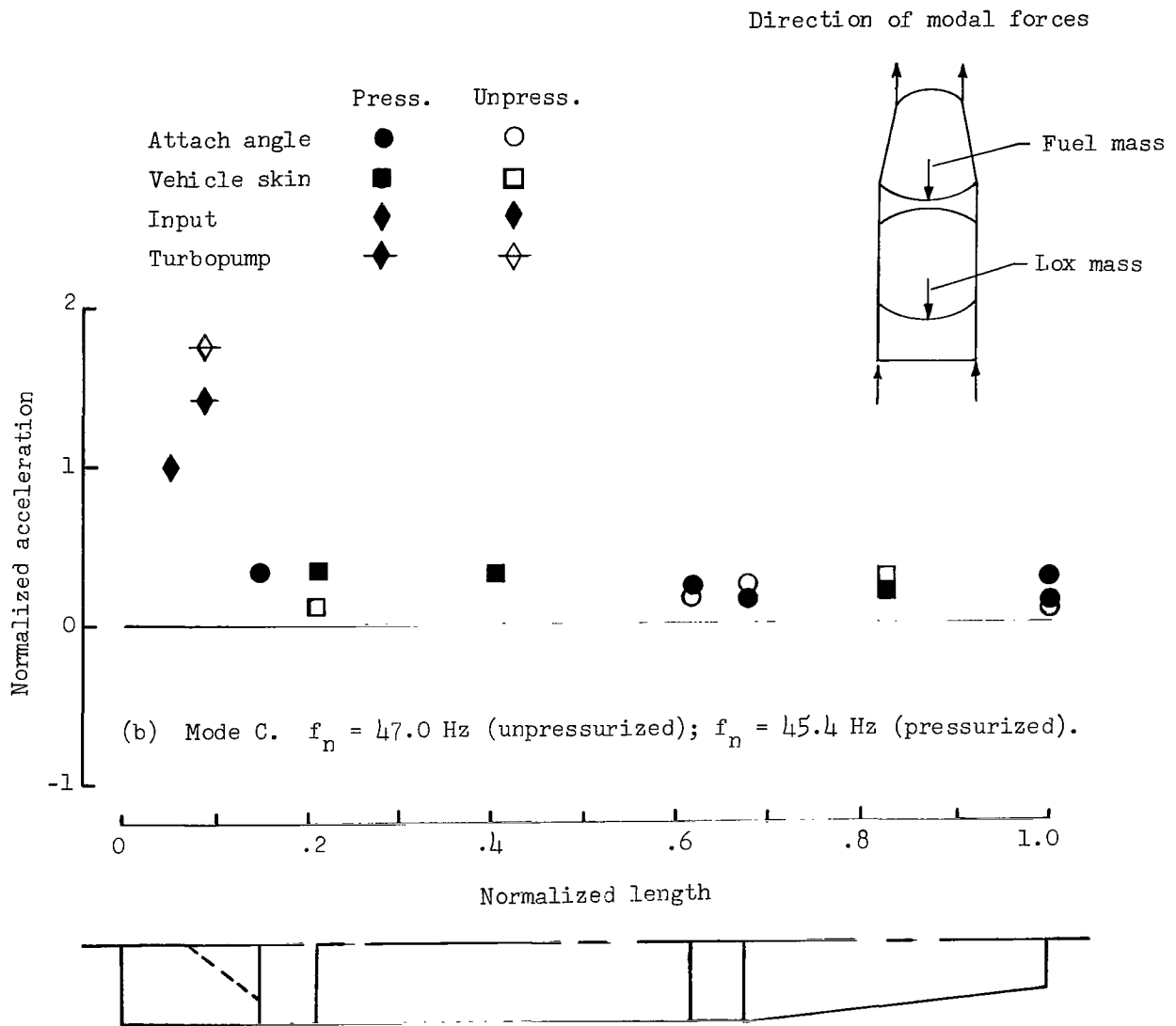


Figure 24.- Concluded.

Direction of modal forces

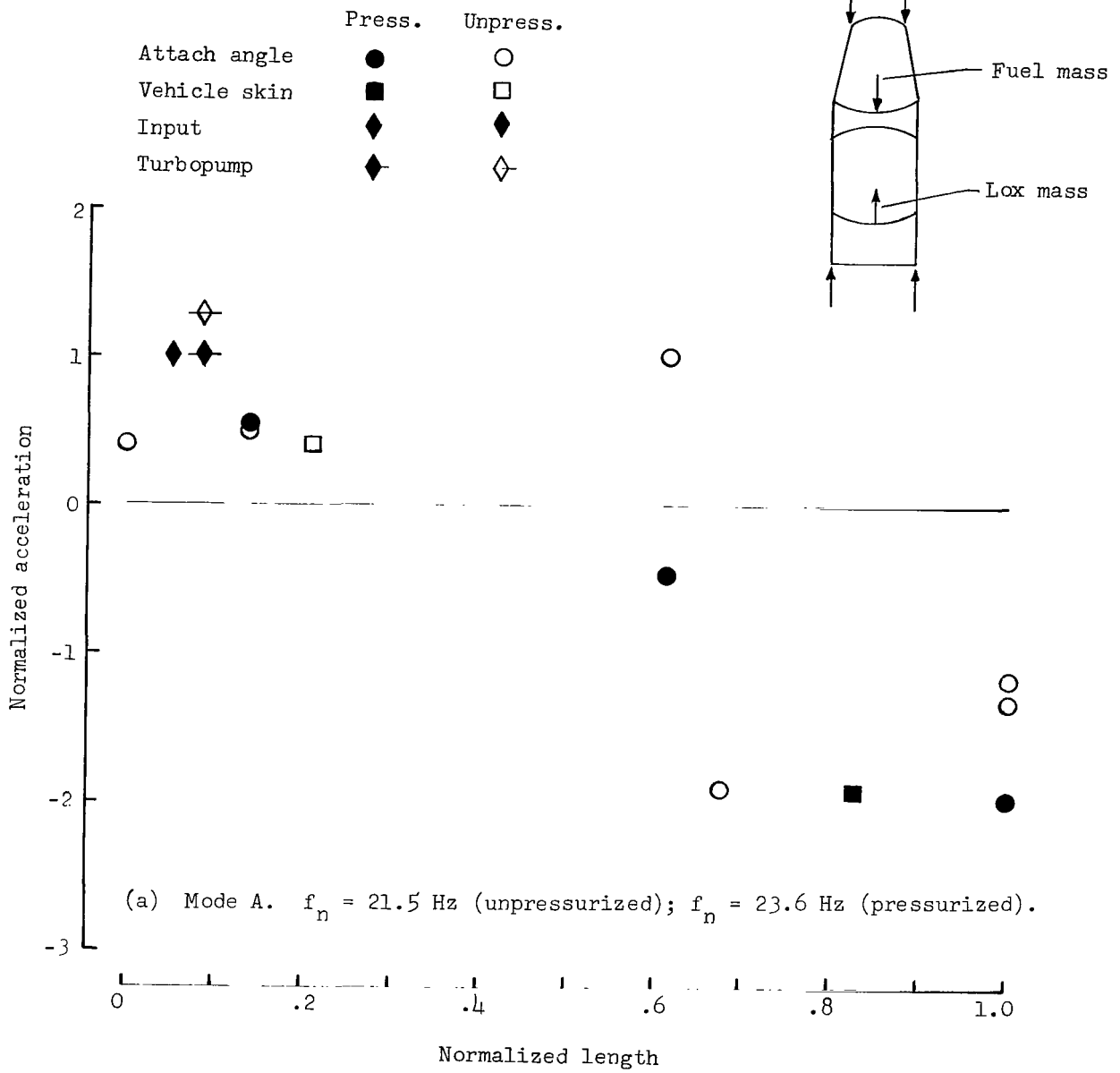


Figure 25.- Resonant response accelerations of vehicle configurations 3 and 3P.

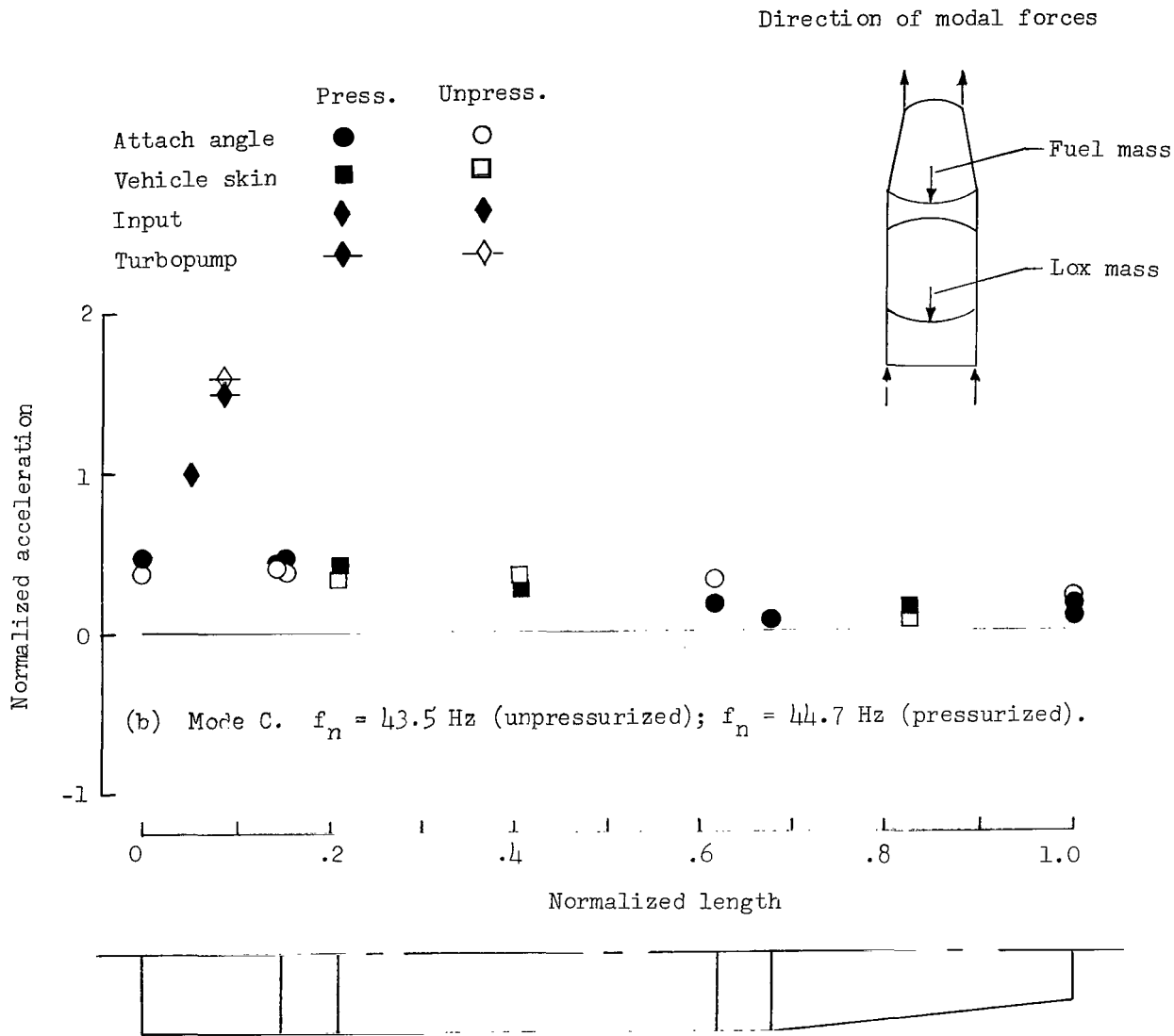


Figure 25.- Concluded.

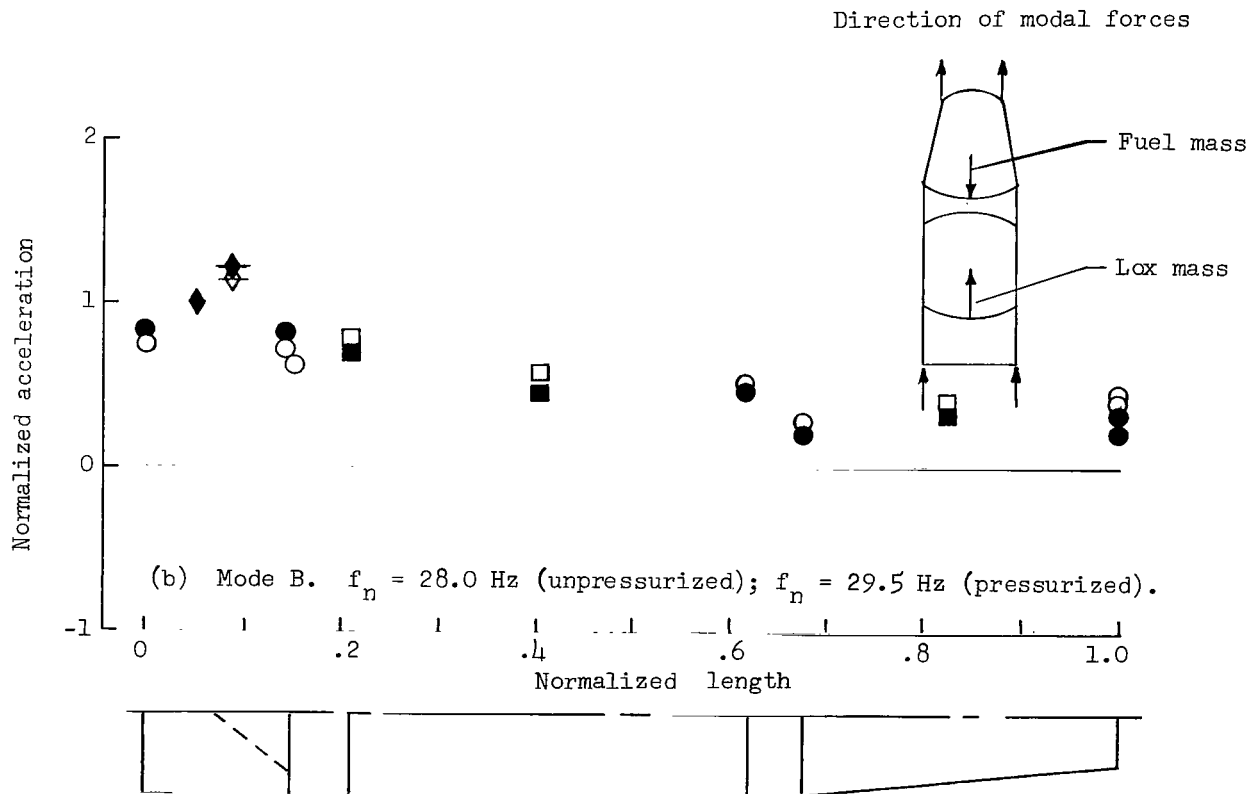
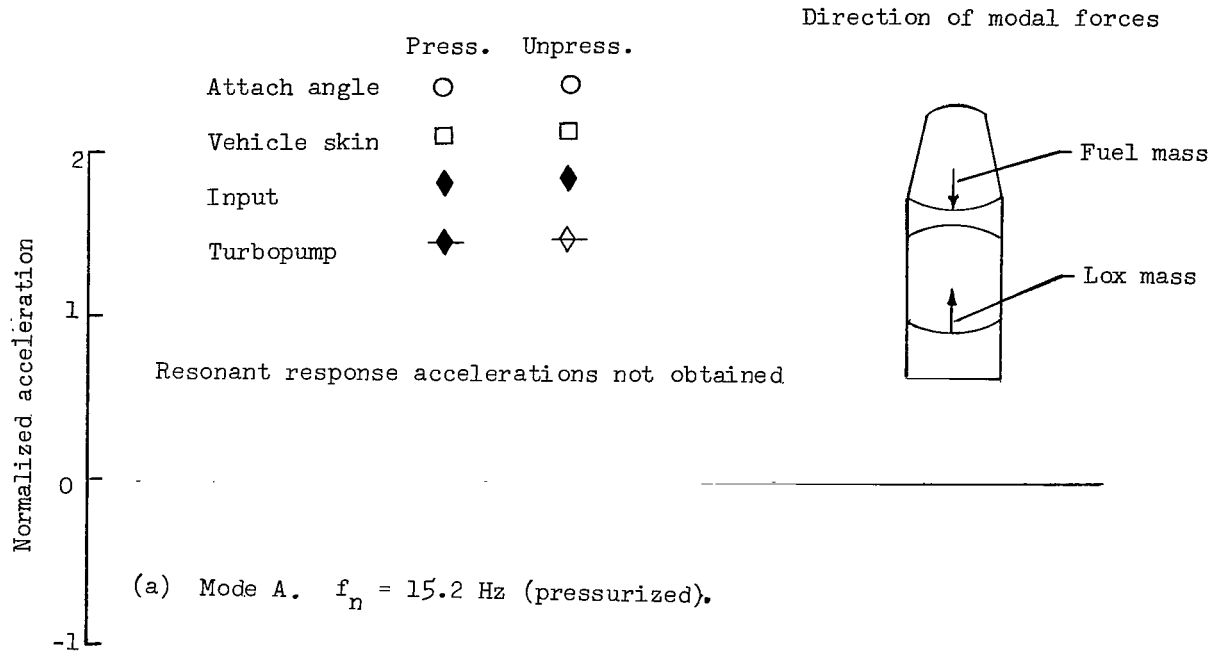


Figure 26.- Resonant response accelerations of vehicle configurations 6 and 6P.

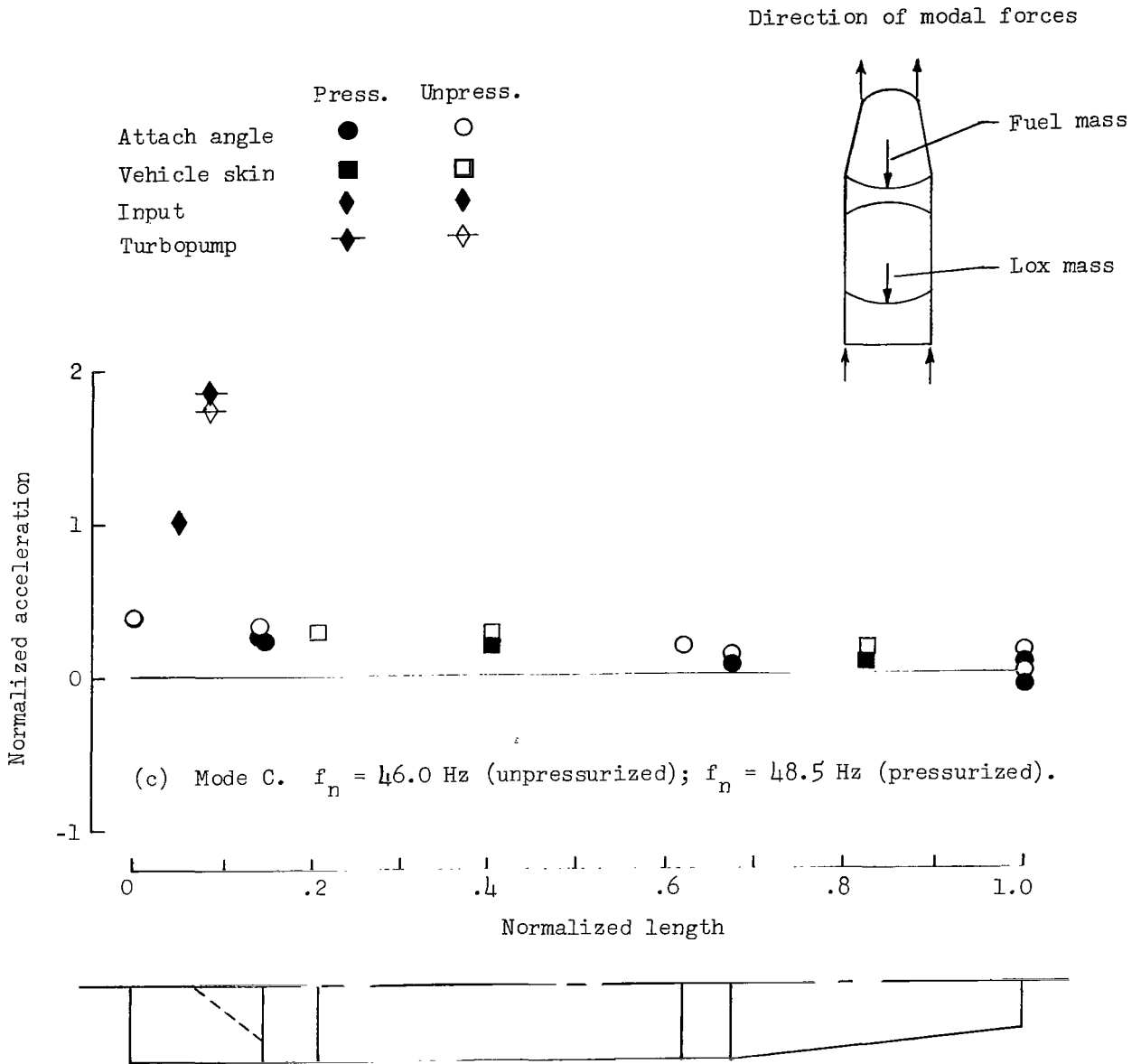


Figure 26.- Concluded.

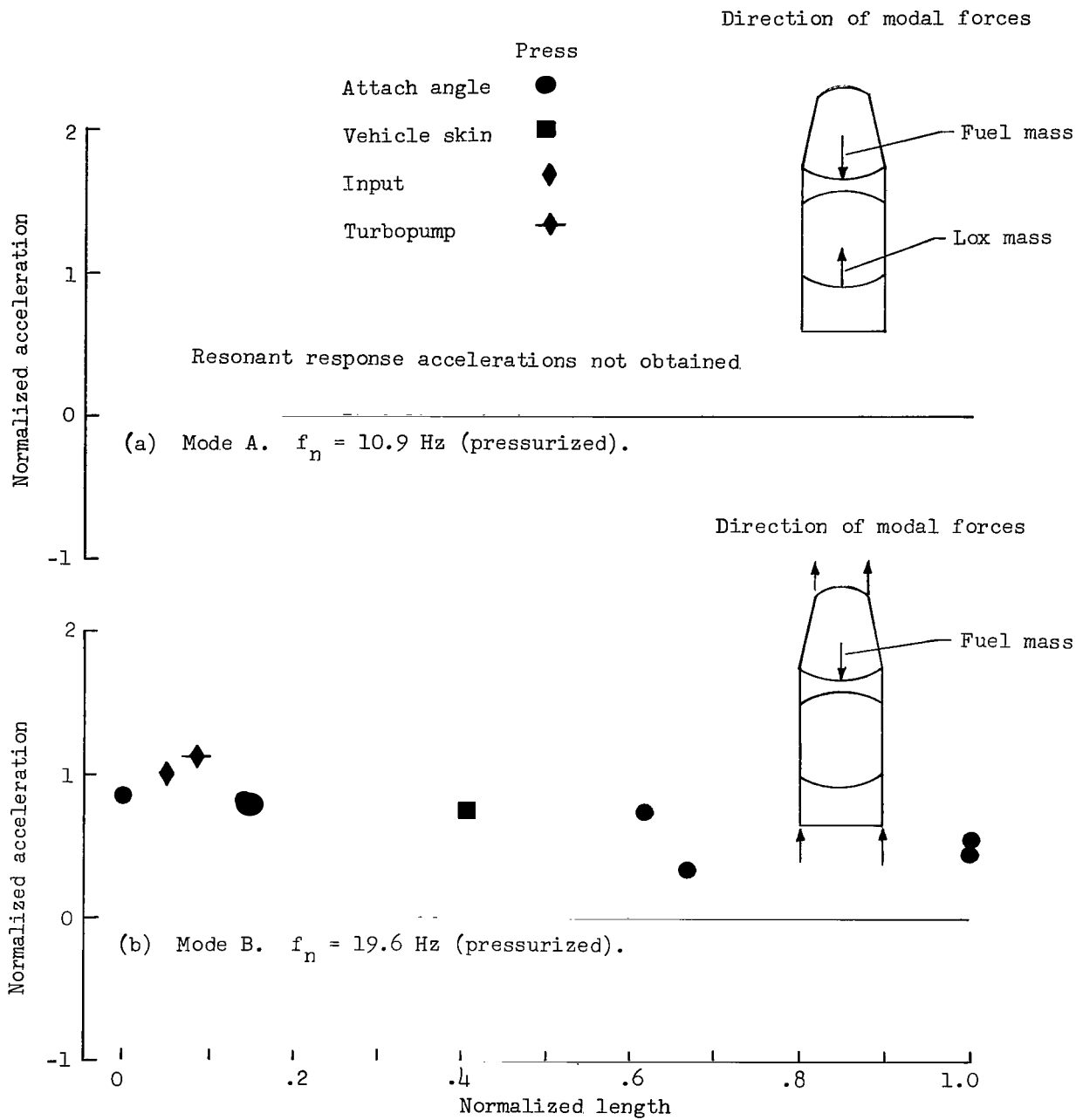


Figure 27.- Resonant response accelerations of vehicle configurations 9 and 9P.

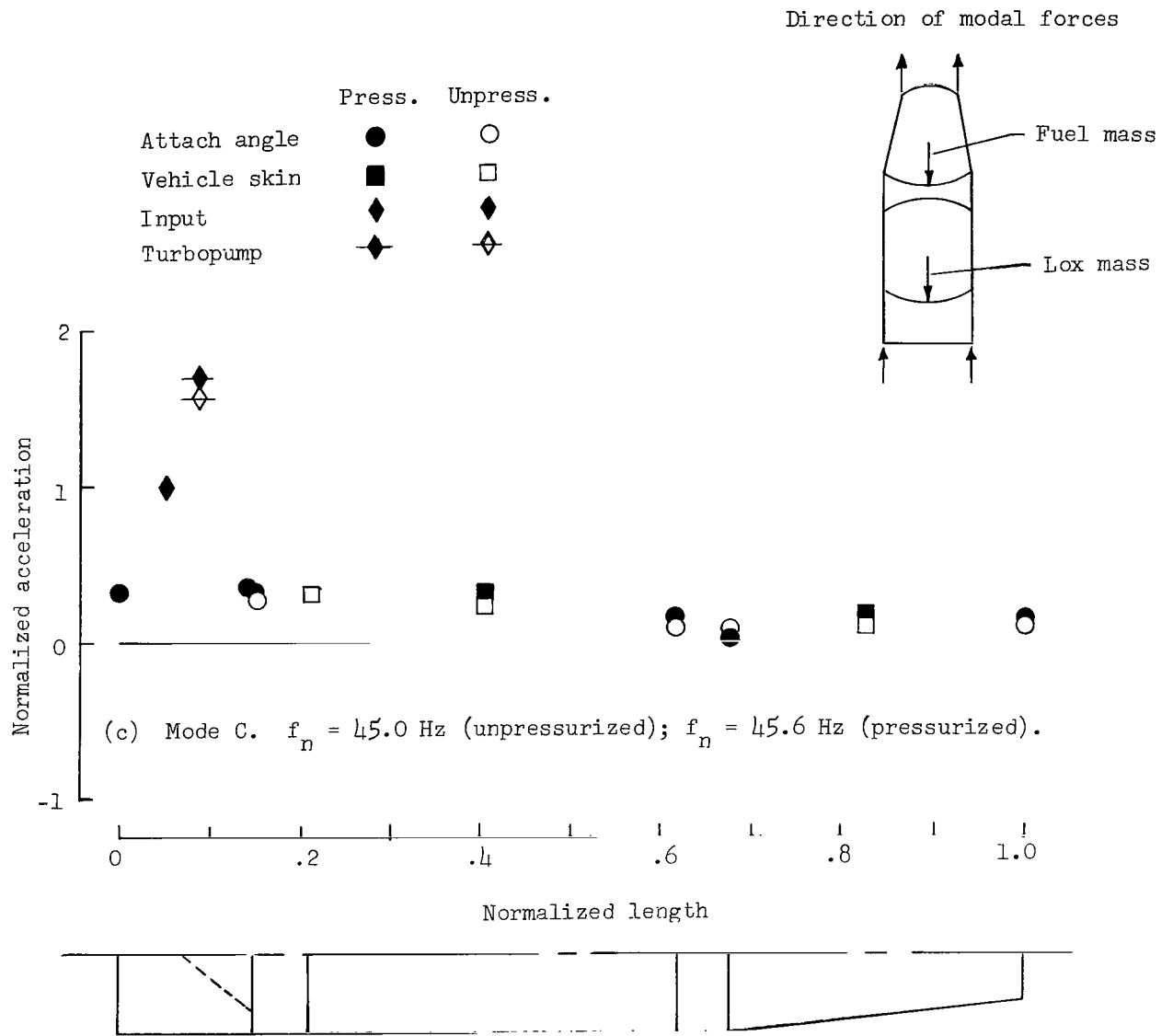
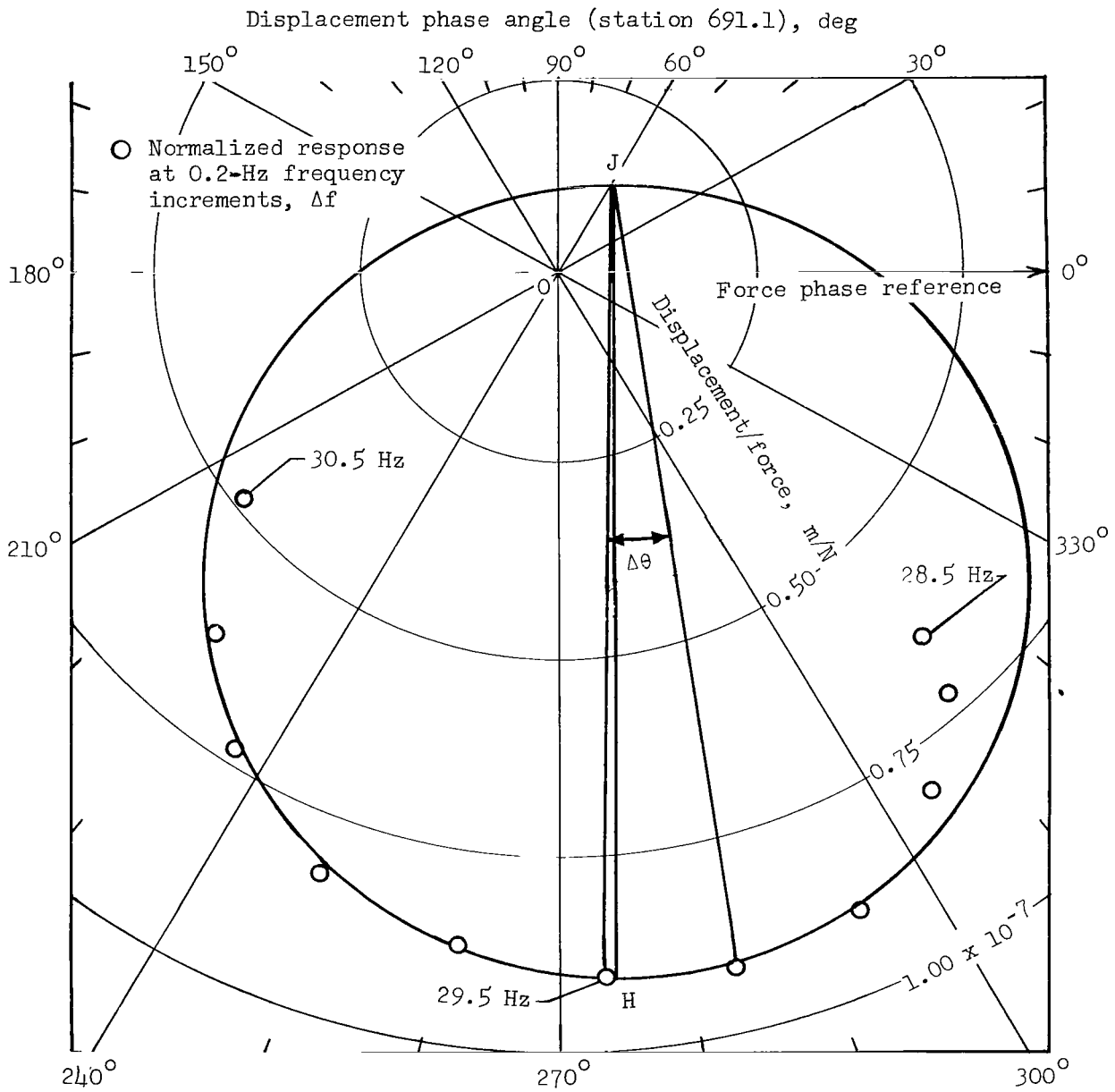


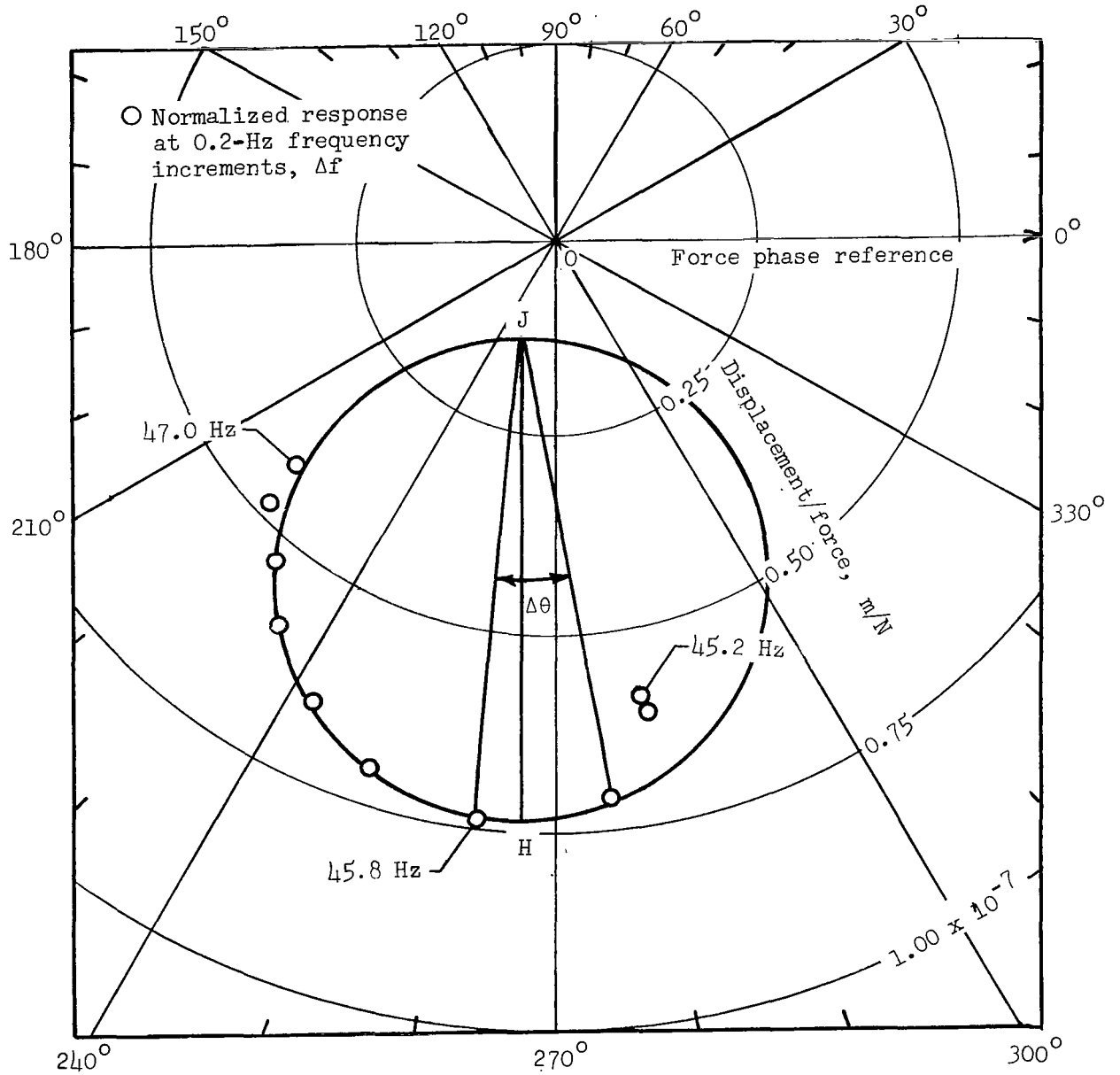
Figure 27.- Concluded.



(a) Mode B. $f_n = 29.5$ Hz; $\mu = 0.08$.

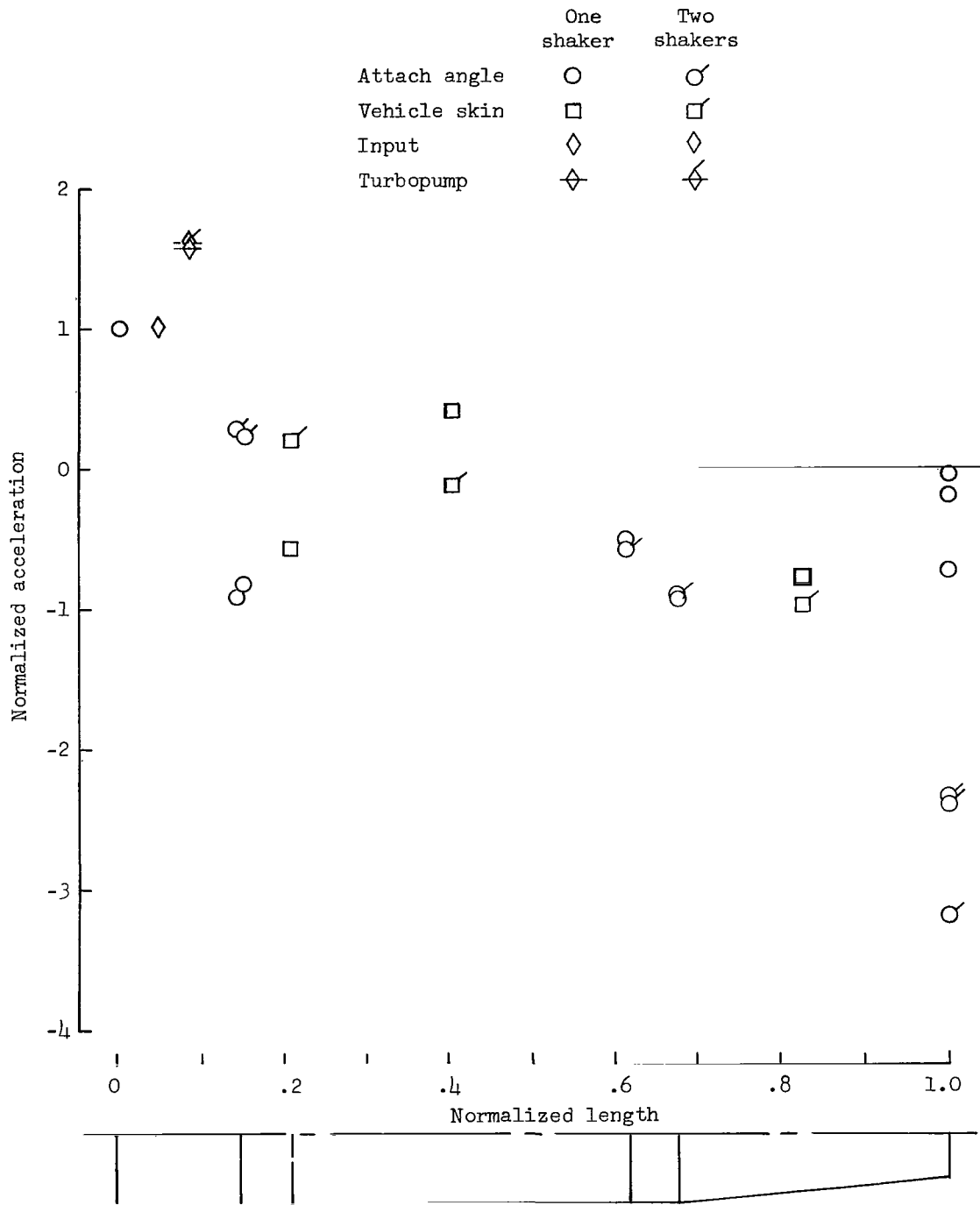
Figure 28.- Kennedy-Pancu plots for modes B and C of configuration 6P.

Displacement phase angle (station 691.1), deg



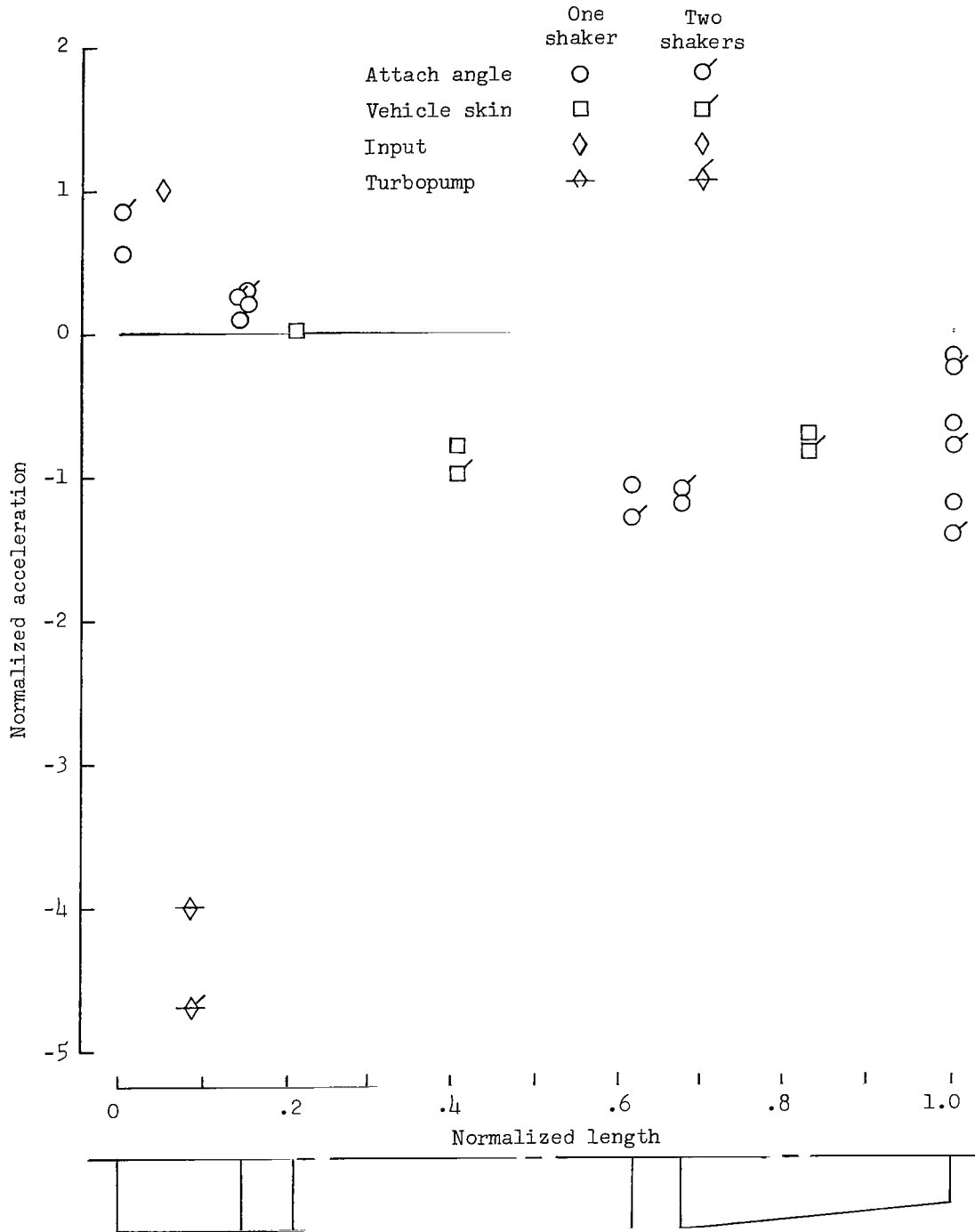
(b) Mode C. $f_n = 45.8$ Hz; $\mu = 0.03$.

Figure 28.- Concluded.



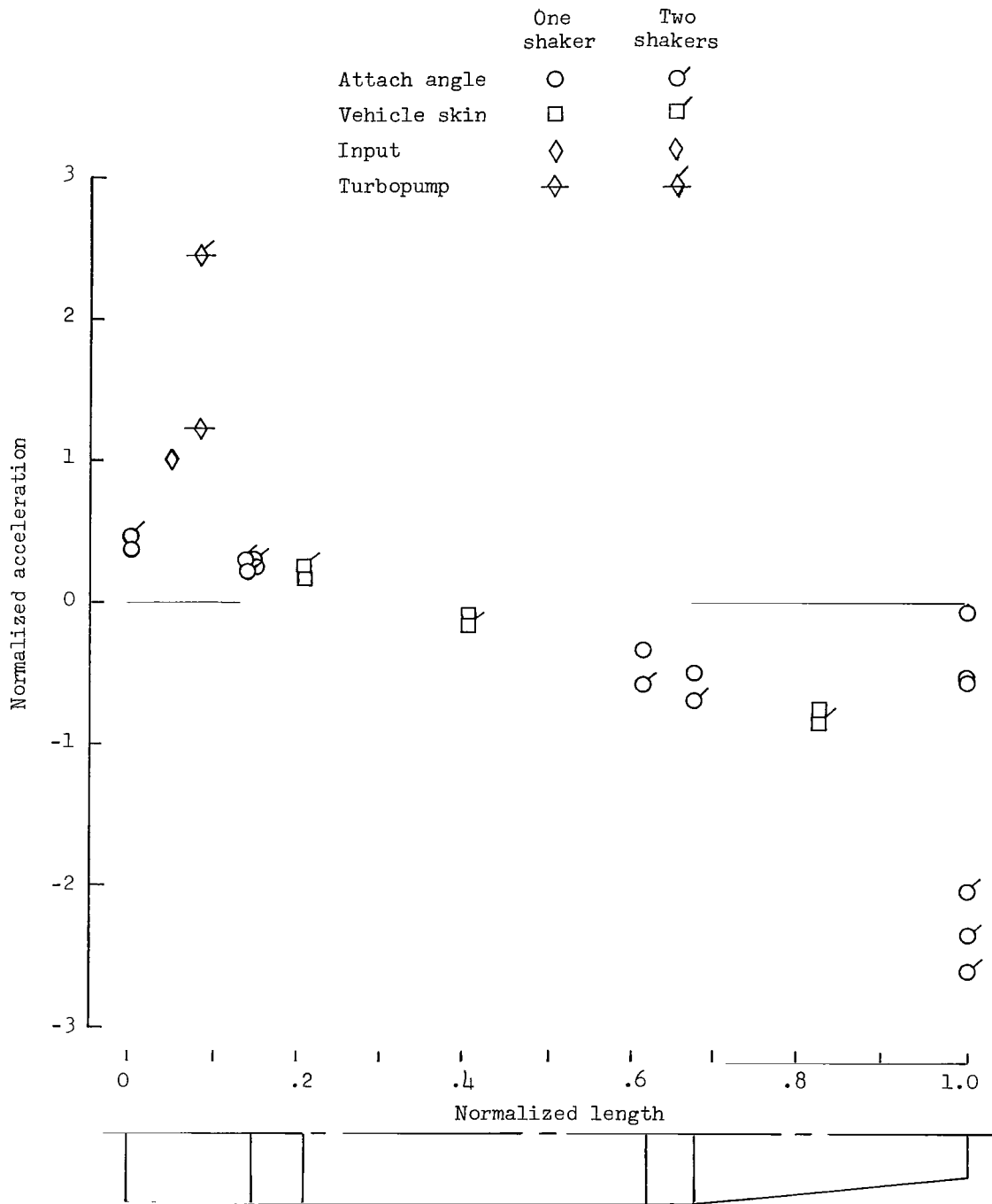
(a) $f_n = 60.3$ Hz (two shakers); $f_n = 60.5$ Hz (one shaker with frame).

Figure 29.- Resonant response accelerations for configuration 1 obtained by using one and two shakers.



(b) $f_n = 81.0$ Hz (two shakers); $f_n = 80.3$ Hz (one shaker with frame).

Figure 29.- Continued.



(c) $f_n = 88.0$ Hz (two shakers); $f_n = 88.0$ Hz (one shaker with frame).

Figure 29.- Concluded.

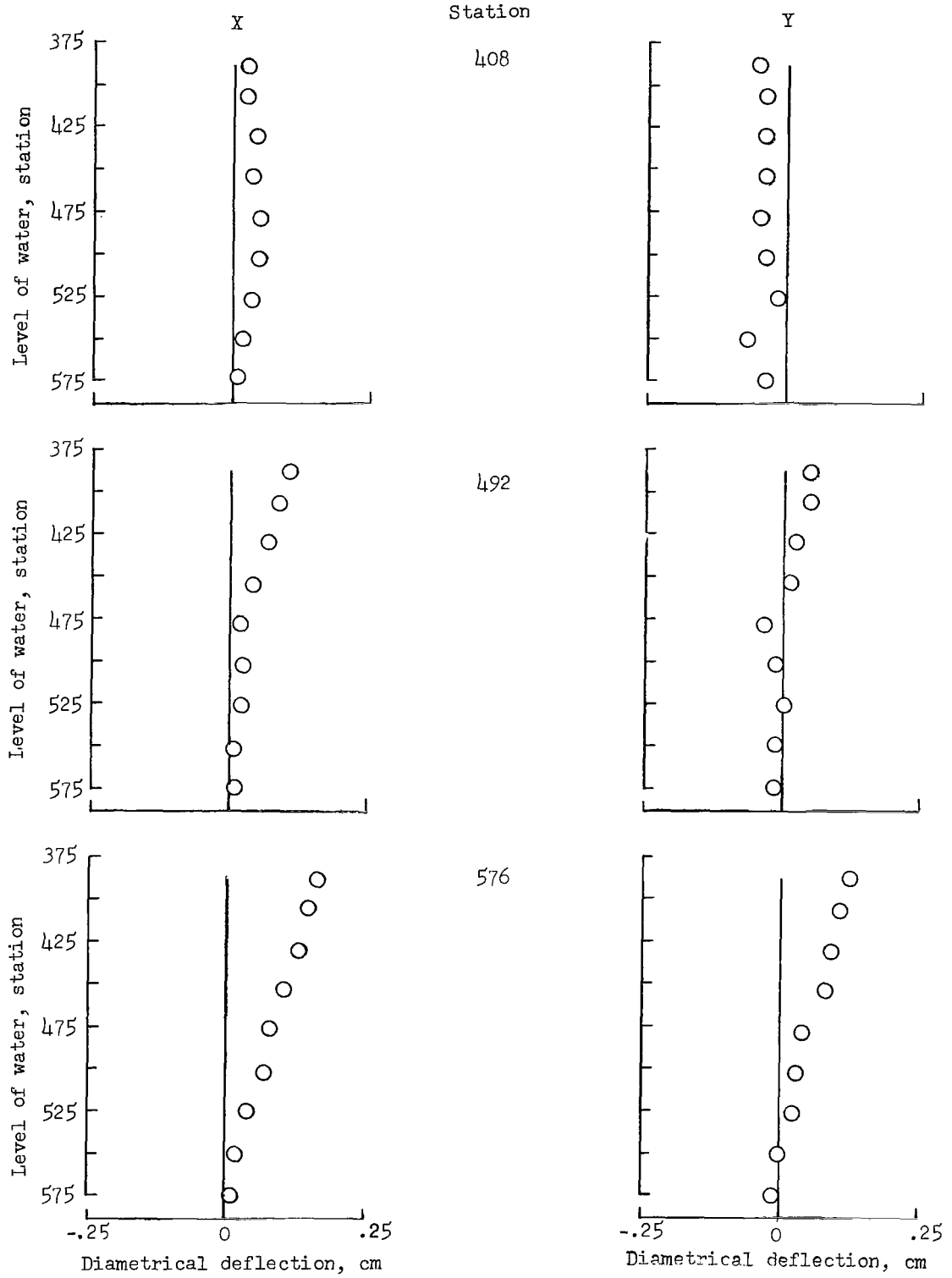


Figure 30.- Increase in vehicle diameter during propellant loading.

| | Increasing mass | Decreasing mass |
|--------------------------|--------------------|--------------------|
| Quarter-point deflection | □ | ◻ |
| Center deflection | ○ | ◉ |

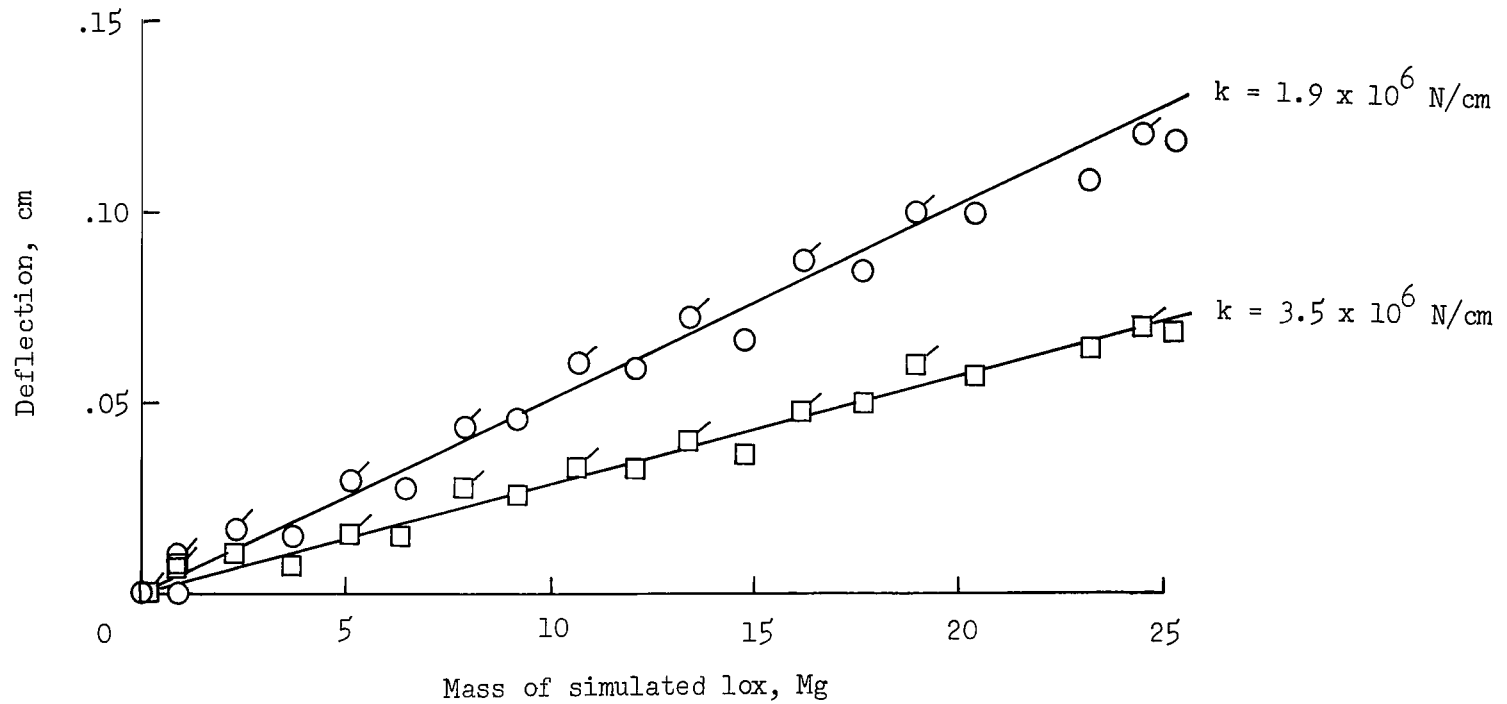


Figure 31.- Static deflection of the bottom bulkhead of the liquid-oxygen tank caused by mass of the simulated propellant.

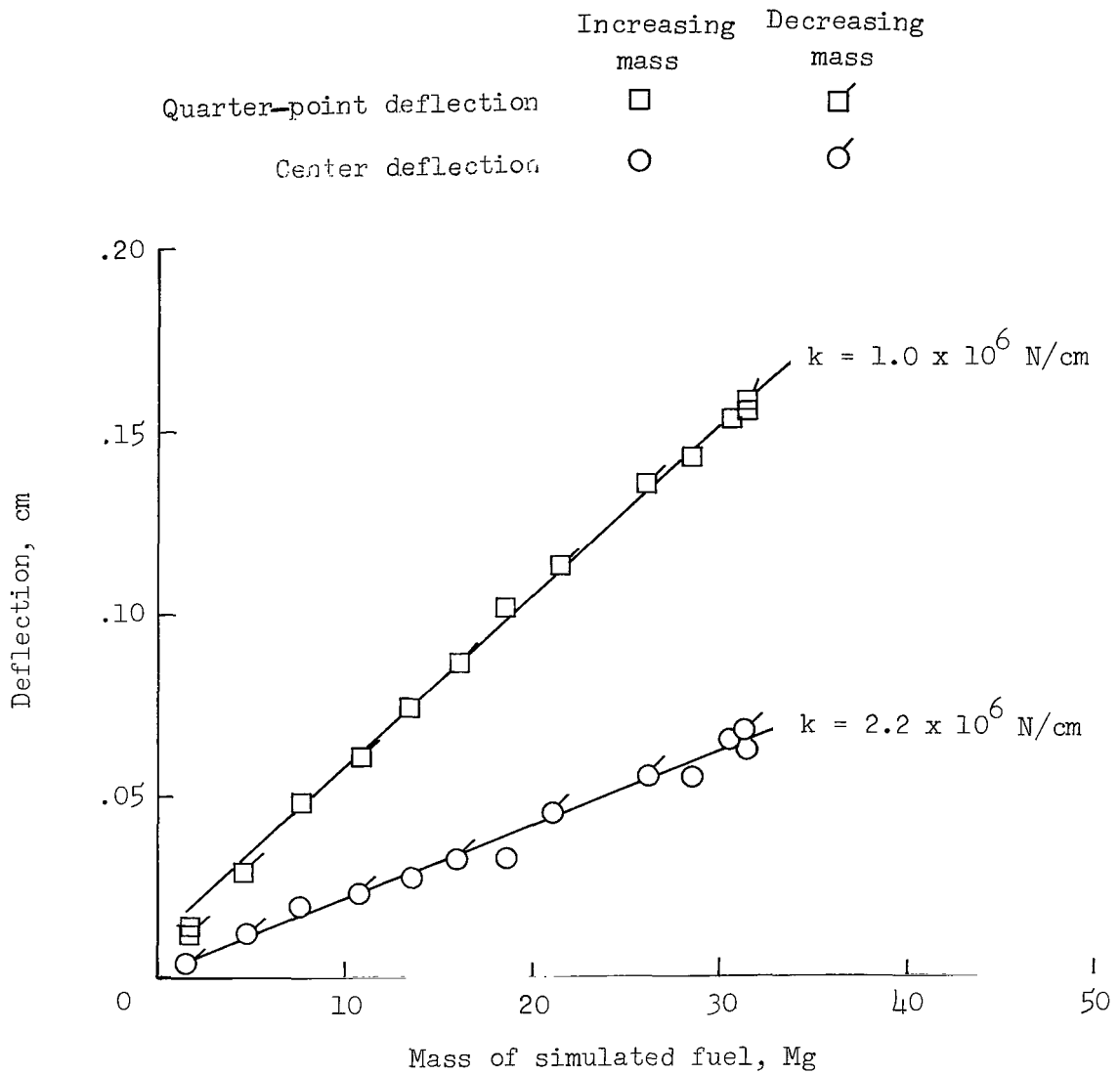


Figure 32.- Static deflection of the bottom bulkhead of the fuel tank caused by mass of the simulated propellant.

FIRST CLASS MAIL

030 001 57 51 3DS 08106 00903
AIR FORCE WEAPONS LABORATORY/AFWL/
KIRTLAND AIR FORCE BASE, NEW MEXICO 87117

ATTN MISS MADELINE F. CALOVA, CHIEF TECHNICAL
LIBRARY /MLIL/

POSTMASTER: If Undeliverable (Section 158
Postal Manual) Do Not Return

"The aeronautical and space activities of the United States shall be conducted so as to contribute . . . to the expansion of human knowledge of phenomena in the atmosphere and space. The Administration shall provide for the widest practicable and appropriate dissemination of information concerning its activities and the results thereof."

— NATIONAL AERONAUTICS AND SPACE ACT OF 1958

NASA SCIENTIFIC AND TECHNICAL PUBLICATIONS

TECHNICAL REPORTS: Scientific and technical information considered important, complete, and a lasting contribution to existing knowledge.

TECHNICAL NOTES: Information less broad in scope but nevertheless of importance as a contribution to existing knowledge.

TECHNICAL MEMORANDUMS: Information receiving limited distribution because of preliminary data, security classification, or other reasons.

CONTRACTOR REPORTS: Scientific and technical information generated under a NASA contract or grant and considered an important contribution to existing knowledge.

TECHNICAL TRANSLATIONS: Information published in a foreign language considered to merit NASA distribution in English.

SPECIAL PUBLICATIONS: Information derived from or of value to NASA activities. Publications include conference proceedings, monographs, data compilations, handbooks, sourcebooks, and special bibliographies.

TECHNOLOGY UTILIZATION PUBLICATIONS: Information on technology used by NASA that may be of particular interest in commercial and other non-aerospace applications. Publications include Tech Briefs, Technology Utilization Reports and Notes, and Technology Surveys.

Details on the availability of these publications may be obtained from:

**SCIENTIFIC AND TECHNICAL INFORMATION DIVISION
NATIONAL AERONAUTICS AND SPACE ADMINISTRATION
Washington, D.C. 20546**